

Corrosion and Inhibition Performances at the Steel-Mortar Interface. Part 1: A Surface Analytical Investigation

Zhengxian Yang¹, Xianming Shi^{1,2,*}, Tuan Anh Nguyen¹, Zhiyong Suo³, Recep Avci³

¹ *Corrosion and Sustainable Infrastructure Laboratory, Western Transportation Institute, PO Box 174250, College of Engineering, Montana State University, Bozeman, MT 59717-4250, USA*

² *Civil Engineering Department, 205 Cobleigh Hall, Montana State University, Bozeman, MT 59717-2220, USA*

³ *Imaging and Chemical Analysis Laboratory, Department of Physics, Montana State University, Bozeman, MT 59717, USA*

* *Corresponding Author; Phone: 1-406-994-6486; Fax: 1-406-994-1697; E-mail: Xianming_s@coe.montana.edu*

Abstract

The present research evaluated the corrosion and inhibition performances of steel-mortar samples with various levels of NaCl and corrosion inhibitors admixed in fresh mortar (0.05M DGP, 0.5M SN, and 0.05M DMEA). FESEM, EDX and XPS were used to analyze the fracture surfaces of the steel-mortar interfacial region for samples exposed to various time periods of ponding by 3% NaCl solution. The admixing of NaCl and the corrosion inhibitors in fresh mortar altered the morphology and microstructure of the hardened mortar at the steel-mortar interfacial region. The admixing of the corrosion inhibitors in fresh mortar increased the risk of carbonation of cement hydrates at the steel-mortar interfacial region, but partially displaced chloride ions. Chloride (either admixed or ingressed) and the admixed corrosion inhibitors facilitated the formation of different cement hydrates and affected chloride binding at the steel-mortar interfacial region, all of which may affect the steel corrosion and its inhibition.

1. Introduction

One of the serious concerns to the durability of reinforced concrete worldwide is chloride-induced corrosion of reinforcing steel ¹⁻³, which leads to a subsequent loss in the strength, serviceability, and aesthetics of the structure. Chloride contamination or chloride ingress into concrete may create the need for early repair or premature substitution of the structure due to steel corrosion ⁴⁻⁶. Such concrete structures include highway concrete slabs, bridge decks and parking garages exposed to chloride-based deicing salts ⁷, structures working in marine environments ⁸⁻⁹, etc.

The use of corrosion inhibitors for new structures, also known as corrosion inhibiting admixtures (CIAs), seems to be a promising strategy in controlling steel corrosion in concrete ¹⁰⁻¹³. Extensive research has been conducted to investigate the mechanisms of steel corrosion in concrete in the presence of aggressive chloride ions, and numerous corrosion inhibitors to mitigate the corrosion of steel in concrete have been studied ¹⁴⁻¹⁸. As the first type of commercial CIAs used to prevent chloride-induced corrosion of embedded steel, nitrites have been known to feature oxidizing properties to inhibit the anodic reaction of the corrosion process ¹⁹⁻²⁰. Among them, sodium nitrite was proven to be a very effective corrosion inhibitor, although its detrimental effects on mortar or concrete strength have been reported ²¹⁻²². Organic CIAs such as amines and esters may successfully inhibit both the anodic and cathodic reactions of corrosion processes, by forming a protective film on the steel surface and thus blocking the access of chlorides as well as oxygen ²³⁻²⁵.

Nonetheless, how CIAs work to control the corrosion of steel in concrete are still not fully understood, when it comes to how they might alter the microstructure and chemistry of

hardened concrete and how such changes might affect the steel corrosion and its inhibition. Furthermore, the field performance of CIAs reported in literature are often inconclusive, which may be attributable to the variability inherent in the suite of other relevant factors such as concrete mix design, construction practices, as well as environmental and mechanical loadings experienced by the concrete structure. These knowledge gaps have hindered the widespread implementation of CIAs as a best practice for corrosion management. More research is thus needed to unravel the role of salt contamination and CIAs in the processes of cement hydration and rebar corrosion.

A majority of the existing research pertinent to steel corrosion in concrete has been carried out with the steel sample either immersed in a simulated pore solution, or embedded in cement mortar or concrete specimens. In the former case, the research findings are of limited value to field applications as such experiments ignore the uniqueness of a concrete environment compared with typical aqueous solution environments. In the latter case, measurements of corrosion characteristics of the steel are indirect. Even if the cement mortar or concrete specimen is broken open and the steel is then taken for analyses, it is difficult to obtain reliable information from the relevant interfacial region considering possible damage or contamination of the steel surface.

In this work, a different model system was designed to facilitate the investigation of the steel-mortar interface, with minimal damage at the interfacial region. Two methods were used in combination to bring the chloride ions into direct contact with the steel: admixing sodium chloride into the fresh mortar, and ponding the hardened mortar in a sodium chloride solution. Three CIAs, sodium nitrite [SN, NaNO_2], disodium β -glycerophosphate [DGP,

C₃H₇Na₂O₆P] and N,N'-dimethylethanolamine [DMEA, (CH₃)₂NCH₂CH₂OH] were investigated.

In this paper (Part 1), we report on using field emission scanning electron microscopy/energy dispersive x-ray spectroscopy (FESEM/EDX) and X-ray photoelectron spectroscopy (XPS) to unravel the role of salt contamination and admixed corrosion inhibitors in the processes of cement hydration and rebar corrosion. In a separate paper (Part 2), we report on using electrochemical impedance spectroscopy (EIS) to characterize the behavior of steel-mortar samples admixed with sodium chloride and corrosion inhibitors²⁶. SEM and EDX provide information on surfaces and thus shed light on the localized morphology and chemistry of cement hydrates at the steel-mortar interfacial region relative to the spatial distribution of steel corrosion products. Recent technological advances in SEM/EDX enable the observation to be performed under a weak vacuum, allowing retention of moisture in the sample. As such, cement hydrates can be studied without suffering from the micro-shrinkage or crystallization due to moisture evaporation²⁷. XPS has been previously utilized to confirm the formation of inhibitor film on the surface of reinforcing steel²⁸.

2. Experimental procedures

2.1. Materials. An ASTM specification C150-07 Type I/II low-alkali Portland cement (ASH Grove Cement Company Clancy, MT) was used in this study. The chemical composition and physical properties of the cement are listed in Tables 1 and 2, respectively. The fine aggregates used were river sand sifted with a 250 μ m sieve before proportioning and admixing. Steel plates (C4130 carbon steel) were purchased from Metal Samples, Inc.

(Munford, AL). De-ionized water was used in the experiment.

2.2. Sample preparation. All the mortar samples were prepared with cement: sand: water mass ratio of 1: 0.075: 0.5. The percentages and concentrations of chloride and inhibitors that were added to the mortar were by weight of water. Table 3 shows the mix design for the six types of samples with various contents of admixed chloride and inhibitors. The chloride contamination levels (3% and 3.8% by weight of water) in fresh mortar were used to simulate the scenarios where seawater is used for concrete mixing and construction for seashore structures and components. For each sample, fresh mortar was poured into a plastic tube (2.2cm² of surface area, 5mm deep) attached to a square steel plate (2.5cm × 2.5cm) using epoxy resin and carefully compacted to minimize air voids. The steel plate was cleaned with de-ionized water and acetone and dried in advance. Following curing in a wet chamber for 28 days at approximately 20°C and 95% relative humidity, each steel-mortar sample was demoulded from the plastic tube and another plastic tube (2.2cm² of surface area, 10mm deep) was sealed on top of it to serve as a reservoir. To initiate steel corrosion, all samples were then ponded with 3% NaCl solution. Three specimens were prepared for each mix design to validate the reliability of test results.

2.3. Surface analyses. After being ponded with the 3% NaCl solution for a given period, each steel-mortar sample was detached from the pond; the steel plate and mortar were then separated mechanically from each other by shear force. The freshly exposed fracture surface on each mortar specimen was then subjected to FESEM/EDX to examine its localized morphology and elemental distributions at the microscopic level, using a Zeiss Supra 55VP PGT/HKL system coupled with the energy dispersive x-ray analyzer. The EDX

data were obtained with a micro-analytical unit that featured the ability to detect the small variations of trace element content. We used FESEM/EDX under variable pressure (VP mode), typically 10^{-2} torr, to investigate the effect of sodium chloride (NaCl) and inhibitors on the morphology and chemistry of cement hydrates at the steel-mortar interfacial region, after ponding by 3% NaCl. The VP mode allowed the analyses of mortar microstructure and cement hydrates without any information distortion seen in traditional SEM.

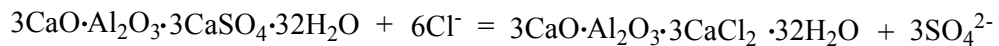
The freshly exposed fracture surface on each steel plate was subjected to XPS to examine its localized chemistry, using a Physical Electronics 5600ci system equipped with monochromatized Al K α X-ray source featuring standard excitation energy of 1486.6eV. Data acquisition and analysis were performed using the RBD AugerScan2 software. After acquiring a typical survey scan, a high resolution scan (multiplex) was conducted to identify individual element peaks of interest. The energy scale was corrected to the C 1s peak maxima at 285eV.

3. Results and discussion

3.1. Morphology and microstructure of hardened mortars at the steel-mortar interfacial region

3.1.1. Effects of admixed NaCl. The admixing of NaCl in fresh mortar was found to alter the morphology and microstructure of the hardened mortar at the steel-mortar interfacial region, as illustrated by the FESEM images of the fracture surface on the mortar samples A, B, and C after being ponded by 3% NaCl solution for 60 days (see Figures 1A-1C, all at magnification level of approximately 500 times). The mortar sample without any chloride

admixed (A) had a relatively homogeneous surface, featuring the presence of fine rod-like AFt phases (calcium aluminate trisulfate hydrates)²⁹. For the samples with 3% and 3.8% NaCl admixed in fresh mortar (B and C), the exfoliated lamella crystals dominated the fracture surface, while delicate globular or whiskery minerals were also observed. The exfoliated lamella crystals were reported to be responsible for expansion and subsequent cracking and spalling of concrete³⁰, which might have aggravated the expansion due to the diffusion of steel corrosion products into mortar at the steel-mortar interfacial region. Relative to the sample A, both the samples B and C gave a more textured fracture surface, featuring the presence of hexagonal platy crystals (AFm phases, calcium aluminate monosulfate hydrates) and less AFt phases (shown as coarser rods)³¹. A possible mechanism responsible for the diminished AFt phases is the substitution of the sulfate anion in AFt phases by the chloride anion, such as the one converting ettringite into calcium chloro-aluminate:



Furthermore, the overall characteristics of the fracture surface on all three mortar samples were consistent with a reticulated Type II C-S-H (calcium silicate hydrates), which was observed in samples with chloride admixed in fresh mortar²⁹.

3.1.2. Effects of admixed corrosion inhibitors. The admixing of corrosion inhibitors in fresh mortar was found to alter the morphology and microstructure of the hardened mortar at the steel-mortar interfacial region, as illustrated by the FESEM images of the fracture surface on the mortar samples D, E, and F after being ponded by 3% NaCl solution for 60 days (see Figures 1D-1F, all at magnification level of approximately 500 times).

Compared with the mortar sample with 3% NaCl but no inhibitors admixed (B), the samples with corrosion inhibitors admixed (D, E, and F) had relatively more homogeneous fracture surfaces. As seen in Figure 1D, the sample with 3% NaCl and 0.05 M DGP admixed in fresh mortar (D) had a coarse mortar fracture surface with many air voids at the steel-mortar interfacial region, which may explain the poor inhibition performance of DGP discussed in our other paper ²⁶. In addition to calcium-rich hexagonal platy crystals (AFm phases), the mortar fracture surface for the sample D featured the presence of spherulites characteristic of a Type I C-S-H, which generally occurred in samples without chloride admixed in fresh mortar ²⁹. This indirectly suggests the displacement of chloride ions by DGP at the steel-mortar interface, as confirmed by the EDX data discussed later. As seen in Figures 1E and 1F, the samples with 3% NaCl and 0.5 M SN or 0.05M DMEA admixed in fresh mortar (E and F respectively) exhibited a more smooth and bare fracture surface with some microcracks but few air voids at the steel-mortar interfacial region, which may explain the good inhibition performances of SN and DMEA discussed in our other paper ²⁶. In addition, the mortar fracture surface for the sample E featured dense calcium-silicon rich structures and the morphology resembling a reticulated Type II C-S-H ²⁹. The dense microstructure of the sample E along with the presence of evident microcracks at the steel-mortar interfacial region indirectly suggests the “*pore blocker*” role played by SN, as confirmed by the electrochemical data discussed in our other paper ²⁶. The mortar fracture surface for the sample F featured the co-existence of rod-like AFt phases, hexagonal platy AFm phases, and a reticulated Type II C-S-H at the steel-mortar interfacial region.

3.2. Localized chemical composition at the steel-mortar interfacial region

3.2.1. XPS analyses. The freshly exposed fracture surface on each steel plate was subjected to XPS to provide data that would supplement the information obtained with the FESEM/EDX regarding the steel-mortar interfacial region. The XPS is known to provide the chemical composition information of the very top surface layer (less than 10nm) of the tested sample ³², in this case, from the steel-mortar interfacial region to the steel surface. The C 1s peak at binding energy of approximately 290eV on the XPS spectra can be attributed to the carbonation products of Portland cement mortar (PCM) such as calcite, because DGP and DMEA do not contain carboxyl groups and thus C 1s signal for the organic inhibitors is smaller than 290eV. The admixing of each of the three corrosion inhibitors in fresh mortar was found to increase the risk of carbonation of cement hydrates at the steel-mortar interfacial region, as illustrated by the C/Ca ratios of the fracture surface on the steel plate of the samples after 60 days of ponding by 3% NaCl solution (see Figure 2a). Compared with the sample B that had no inhibitors admixed, the samples D, E and F with their respective inhibitor (0.05M DGP, 0.5M SN, and 0.05M DMEA) admixed featured significantly higher C/Ca ratios, signifying the uptake of more atmospheric carbon dioxide by the residual cement hydrates at the fracture surface on the steel plate of these samples. The potential carbonation of cement hydrates may enhance the risk of rebar corrosion in concrete, which is a side effect of these CIAs to be considered in future research and applications. Relative to the sample B, the samples D, E, and F exhibited lower Cl contents at the fracture surface on the steel plate (see Figure 2b), suggesting the partial displacement of chloride ions by the formation of oxide film (in the case of SN) or the chemisorption of organic CIAs (in the case of DGP and DMEA) on the steel surface.

3.2.2. EDX analyses. Using an appropriate accelerating voltage (20KV), the EDX data provided the chemical composition at a large volume, as in the depth of approximately $1\mu\text{m}$ from the steel-mortar interfacial region to the mortar bulk matrix. The EDX data were taken from at least three different sites with high Fe signal (“rusty sites”) and at least three different sites with low Fe signal (“non-rusty sites”) on the fracture surface of each mortar sample at the steel-mortar interfacial region. Each site corresponded to a selected area of approximately $40\mu\text{m} \times 40\mu\text{m}$ (see frames shown in Figures 1A-1F).

The EDX data obtained from the mortar fracture surface of various samples confirm the presence of each of the three CIAs at the steel-mortar interfacial region. For the sample D after 60 days of salt ponding, the EDX data confirm the presence of the inhibitor DGP on the mortar fracture surface, with a phosphorus concentration of 0-0.05 wt.% at rusty sites and 0.14-0.2 wt.% at non-rusty sites. This implies that if DGP had been admixed at a higher content than 0.05M (by weight of mixing water) in fresh mortar, it could have achieved better performance in inhibiting the steel corrosion. For the samples E and F after 60 days of salt ponding, the EDX data confirm the presence of the inhibitors SN and DMEA at the steel-mortar interfacial region, with an average nitrogen concentration of 0.45 wt.% and 0.81 wt.% on their mortar fracture surfaces respectively.

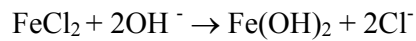
Figure 3 illustrates the evolution of Cl/Ca (a) and N/Ca (b) elemental ratio of the fracture surface on various mortar samples during the 180-day ponding by 3% NaCl solution, with data averaged for EDX measurements taken from three rusty sites and three non-rusty sites on each sample. Throughout the duration of salt ponding, for the samples without any inhibitor admixed (A, B, and C), the rusty sites on the mortar fracture surface

exhibited higher Cl/Ca ratios than the non-rusty sites (see Figure 3a), which confirms the role of chloride ions in causing the steel corrosion. In general, the samples with more NaCl admixed in fresh mortar were found to exhibit higher Cl/Ca ratios (see Figure 3a), which indirectly demonstrates the validity of the EDX technique in characterizing the localized chemistry of the mortar fracture surface.

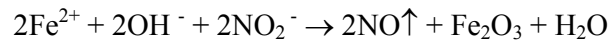
The N/Ca ratios from rusty sites and non-rusty sites on the mortar fracture surface as shown in Figure 3b are expected to illustrate the distribution of DEMA and SN at the steel-mortar interfacial region. For the sample with 3% NaCl and 0.05M DMEA admixed in fresh mortar (F), the non-rusty sites exhibited higher N/Ca ratios than the rusty sites, indicating that higher content of DMEA at the non-rusty sites inhibited the corrosion of steel more effectively, likely through the formation of a more reliable protective film on the steel surface. For the sample with 3% NaCl and 0.5M SN admixed in fresh mortar (E), the non-rusty sites exhibited N/Ca ratios similar to the rusty sites, indicating the uniform distribution of NO_2^- in the hardened mortar, at least in the vicinity of the steel-mortar interface. It is interesting to note that for both the samples E and F, the N/Ca ratio of the mortar fracture surface increased with the time of salt ponding, suggesting the tendency for NO_2^- and DMEA to migrate towards the steel surface from the mortar bulk to control the propagation of chloride-induced corrosion of the steel.

Figure 4 shows the Na/Ca, C/Ca, Al/Ca, S/Al and Si/Ca elemental ratios of the fracture surface on various mortar samples over the 180-day ponding by 3% NaCl solution, with data averaged for EDX measurements taken at day 0, day 60 and day 180. The Na/Ca ratios from rusty sites and non-rusty sites on the mortar fracture surface as shown in Figure 4a are

expected to shed some light on the steel corrosion and inhibition mechanisms, even though the sodium signal could be derived from either NaCl or inhibitors (DGP and SN respectively). For the samples without any inhibitor admixed (A, B, and C), the rusty sites on the mortar fracture surface exhibited similar time-averaged Na/Ca ratio (see Figure 4a) but higher Cl/Ca ratios (see Figure 3a) than the non-rusty sites, which is consistent with known mechanisms of chloride-induced corrosion of steel ⁵:



The samples with more NaCl admixed in fresh mortar were found to exhibit higher Na/Ca ratios (see Figure 4a), which confirms the validity of the EDX technique. For the sample with 3% NaCl and 0.05M DGP admixed in fresh mortar (D), its non-rusty sites exhibited significantly higher time-averaged Na/Ca ratio than the rusty sites, suggesting that higher DGP content at the non-rusty sites led to better inhibition performance. For the sample with 3% NaCl and 0.5M SN admixed in fresh mortar (E), the “rusty sites” (with strong Fe signal) exhibited significantly higher time-averaged Na/Ca ratio than the “non-rusty sites” (see Figure 4a), which may be explained by the similar diffusion behavior of ferrous ions and sodium ions. This observation is consistent with the known inhibition reaction characteristic of nitrites ³³:



For the sample with 3% NaCl and 0.05M DMEA admixed in fresh mortar (F), both its rusty and non-rusty sites exhibited significantly lower Na/Ca ratios than the sample without any inhibitor admixed (B), which along with the lower Cl signal observed in XPS (see Figure

2b) suggest the partial displacement of Na^+ as well as Cl^- by DMEA from the steel-mortar interfacial region.

The C/Ca ratios from rusty sites and non-rusty sites on the mortar fracture surface as shown in Figure 4b are expected to shed some light on the steel corrosion and inhibition mechanisms, even though the carbon signal could be derived from either the carbonation products of cement mortar or inhibitors (DGP and DMEA respectively). For the samples without any inhibitor admixed (A, B, and C), the rusty sites on the mortar fracture surface exhibited relatively higher time-averaged C/Ca ratio than the non-rusty sites, which confirms the role of mortar carbonation in aggravating the steel corrosion. The carbonation of mortar hydrates is known to reduce the pH of the pore solution, which may decrease the threshold chloride-to-hydroxyl concentration ratio for the initiation of steel corrosion⁵. The pH reduction may also release some of the bound chlorides (calcium chloro-aluminates, e.g., Friedel's salt) from the mortar matrix³⁴ and thus promote the chloride-induced steel corrosion. For the sample with 3% NaCl and 0.05M DGP admixed in fresh mortar (D), its non-rusty sites exhibited significantly higher time-averaged C/Ca ratio than the rusty sites, likely attributable to the presence of higher content of DGP at the non-rusty sites. For the sample with 3% NaCl and 0.5M SN admixed in fresh mortar (E), the "rusty sites" (with strong Fe signal) exhibited significantly higher time-averaged C/Ca ratio than the "non-rusty sites" (see Figure 4b). A possible explanation is that the presence of more SN in certain areas at the steel-mortar interface led to the uptake of more atmospheric carbon dioxide by cement hydrates, initiated the corrosion of steel and eventually led to the formation of more protective ferric oxide layer in these areas featuring stronger Fe signals.

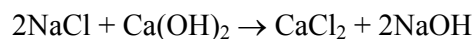
For the sample with 3% NaCl and 0.05M DMEA admixed in fresh mortar (F), the rusty sites had lower content of DMEA (as suggested by the N/Ca ratio shown in Figure 3b) but higher level of mortar carbonation than the non-rusty sites, the combined effects of which led to a relatively higher time-averaged C/Ca ratio at the rusty sites.

The Al/Ca and S/Al ratios on the fracture surface of various mortar samples are shown in Figure 4c and Figure 4d respectively. For all the samples investigated (with or without inhibitor admixed), the rusty sites on the mortar fracture surface consistently exhibited higher time-averaged Al/Ca ratio than the non-rusty sites (see Figure 4c), suggesting the presence of higher content of aluminum-rich cement hydrates. In the absence of inhibitors (samples A, B, and C), the samples with more NaCl admixed in fresh mortar were found to exhibit higher Al/Ca ratios (see Figure 4c) and lower S/Al ratios (see Figure 4d), which along with the low S/Al values suggest the role of admixed chloride in facilitating the formation of more AFm phases in cement hydrates and the partial substitution of the sulfate anion in AFm or AFt phases by the chloride anion (i.e., chloride binding). For the samples without any inhibitor admixed (A, B, and C), the rusty sites on the mortar fracture surface exhibited lower time-averaged S/Al ratio than the non-rusty sites (see Figure 4d), which along with the FESEM images (see Figure 1) and Al/Ca data confirm that the presence of more chloride at the rusty sites at the steel-mortar interface led to the formation of more AFm phases and less AFt phases. The EDX data obtained from the rusty sites also showed the increase of Al/Ca ratio and the decrease of S/Al ratio over time of the 180-day salt ponding for each sample (A, B, and C respectively), indicating both the substitution of AFt phases by AFm phases and the aforementioned chloride binding facilitated by the chloride ions.

Compared with the sample B that had no inhibitors admixed, the admixing of 0.05M DGP in fresh mortar (sample D) led to significantly higher Al/Ca and S/Al ratios in the hardened mortar (at both rusty and non-rusty sites), which along with the high S/Al values suggest that DGP promoted the formation of more aluminum-rich cement hydrates but inhibited the aforementioned chloride binding (possibly due to the displacement of chloride ions by DGP). For the sample D, the rusty sites exhibited higher time-averaged Al/Ca, S/Ca, and S/Al ratios than the non-rusty sites, suggesting that the presence of more AFt phases and their role in facilitating the steel corrosion. For the sample with 3% NaCl and 0.5M SN admixed in fresh mortar (E), its “rusty sites” (with strong Fe signal) featured significantly higher Al/Ca ratios but comparable S/Al ratios than those of sample B, which along with the S/Ca data suggest that with the aid of ferrous ions, SN promoted the substitution of AFt phases by AFm phases but inhibited the aforementioned chloride binding. Compared with the sample B that had no inhibitors admixed, the admixing of 0.05M DMEA in fresh mortar (sample F) led to significantly lower S/Al ratios as well as lower S/Ca ratios, which along with the Al/Ca data suggest that DMEA promoted the substitution of the sulfate anion in AFm or AFt phases by the chloride anion (i.e., chloride binding). Similar to the sample D, the sample F exhibited higher time-averaged Al/Ca, S/Ca, and S/Al ratios at the rusty sites than those at the non-rusty sites, suggesting that the presence of more AFt phases and their role in facilitating the steel corrosion.

The Si/Ca ratios from rusty sites and non-rusty sites on the mortar fracture surface as shown in Figure 4e are expected to shed some light on the role of cement chemistry in the steel corrosion and inhibition processes. The Si/Ca ratio was extensively studied by some

other authors to evaluate the C-S-H phases in cement mortar and concrete^{35,36}. Generally, the Si/Ca ratio of C-S-H phases is somewhat variable with a mean of approximately 0.45-0.55, and C-S-H phases are regarded as the main source of concrete strength and transport properties^{37,38}. For all the samples investigated (with or without inhibitor admixed), the Si/Ca ratio of the mortar fracture surface decreased with the time of salt ponding, implying the substitution of silicate-rich C-S-H by calcium-rich C-S-H facilitated by the chloride ions. For the samples without any inhibitor admixed (A, B, and C), the rusty sites on the mortar fracture surface exhibited relatively lower time-averaged Si/Ca ratio than the non-rusty sites, suggesting the beneficial role of silicate-rich C-S-H phases in controlling the steel corrosion. The admixed chloride seemed to have two competing effects on the Si/Ca ratio. While chloride ions were expected to induce pore refinement and subsequently decrease the Si/Ca ratio of C-S-H phases in mortars³⁹, once sufficient NaCl in the pore solution became available, they might result in the dissolution of Ca(OH)₂ through the following reaction and thus increase the Si/Ca ratio:



Compared with the sample B that had no inhibitors admixed, the admixing of 0.05M DGP in fresh mortar (sample D) led to significantly higher Si/Ca ratios in the hardened mortar (at both rusty and non-rusty sites), suggesting that DGP promoted the formation of more silicate-rich C-S-H phases. This is consistent with the FESEM observations of the sample D and the sample B, which featured the spherulite-like Type I C-S-H (with high Si/Ca ratio²⁹) and the reticulated Type II C-S-H (with low Si/Ca ratio²⁹) respectively, as shown in Figure 1. For the sample D, the rusty sites exhibited lower time-averaged Si/Ca

ratio than the non-rusty sites, suggesting the beneficial role of silicate-rich C-S-H phases in controlling the steel corrosion. Relative to the sample B, the admixing of 0.5M SN in fresh mortar (sample E) led to higher Si/Ca ratios in the hardened mortar (at both rusty and non-rusty sites), suggesting that SN promoted the formation of more silicate-rich C-S-H phases. It is interesting to note that the sample E exhibited slightly higher Si/Ca ratios at its “rusty sites” (with strong Fe signal) than the “non-rusty sites”, attributable to the slightly higher content of SN at the “rusty sites”. Relative to the sample B, the admixing of 0.05M DMEA in fresh mortar (sample F) led to significantly lower Si/Ca ratios in the hardened mortar (at both rusty and non-rusty sites), likely due to the formation of more AFt or AFm phases.

4. Conclusions

With respect to the investigated conditions of steel corrosion, the present research evaluated the changed properties of the interfacial region of steel-mortar systems such as morphology, crystallinity of the cement hydration products and the influence resulting from the admixed sodium chloride and three inhibitors (0.05M DGP, 0.5M SN, and 0.05M DMEA). Surface analytical tools including FESEM/EDX and XPS were used to analyze the fracture surfaces of the steel-mortar interfacial region for samples exposed to various time periods of ponding by 3% NaCl solution.

The FESEM data suggest that the admixing of NaCl and corrosion inhibitors in fresh mortar altered the morphology and microstructure of the hardened mortar at the steel-mortar interfacial region. The XPS data indicate that the admixing of each of the three corrosion

inhibitors in fresh mortar increased the risk of carbonation of cement hydrates at the steel-mortar interfacial region but partially displaced chloride ions from the steel surface.

The EDX data obtained from the freshly exposed mortar fracture surface of various samples confirm the presence of each of the three inhibitors at the steel-mortar interfacial region. We further analyzed the evolution of several critical elemental ratios (Cl/Ca, N/Ca, Na/Ca, C/Ca, Al/Ca, S/Al, and Si/Ca) of the fracture surface on various mortar samples during the 180-day ponding by 3% NaCl solution. The EDX data were taken from three rusty sites (with strong Fe signal) and three non-rusty sites respectively on each sample. The Cl/Ca and C/Ca data confirmed the role of chloride ions and mortar carbonation in causing and aggravating the steel corrosion respectively. Higher content of DGP or DMEA was found to coincide with local areas of less corrosion products on the mortar fracture surface, indicating their better inhibition performances. For SN, the EDX data were consistent with the known passivation reaction characteristic of nitrites. We also found the tendency for NO_2^- and DMEA to migrate towards the steel surface from the mortar bulk to control the propagation of chloride-induced corrosion of the steel. DMEA was found to partially displace both Na^+ and Cl^- from the steel-mortar interfacial region.

The EDX data at the steel-mortar interfacial region suggested the role of chloride (either admixed or ingressed) in facilitating the formation of more AFm phases, the partial substitution of the sulfate anion in AFm or AFt phases by the chloride anion (i.e., chloride binding), and the substitution of silicate-rich C-S-H by calcium-rich C-S-H. DGP promoted the formation of more silicate-rich C-S-H phases that were beneficial in controlling the steel corrosion as well as the formation of more aluminum-rich cement hydrates, but inhibited the

aforementioned chloride binding. The data from the sample with DGP admixed also suggested the role of AFt phases in facilitating the steel corrosion. SN promoted the formation of more silicate-rich C-S-H phases. With the aid of ferrous ions, SN also promoted the substitution of AFt phases by AFm phases but inhibited the aforementioned chloride binding. DMEA promoted the substitution of the sulfate anion in AFm or AFt phases by the chloride anion (i.e., chloride binding) as well as the formation of more AFt or AFm phases.

This work provided improved understanding of the role of admixed chloride and inhibitors in the cement hydration and steel corrosion, which is expected to contribute to the effort of searching for effective measures to mitigate steel corrosion in concrete and protect reinforced concrete structures in a chloride-laden environment.

Acknowledgements

This work was supported by the Research and Innovative Technology Administration under the U.S. Department of Transportation through the University Transportation Center research grant. We would also like to extend our appreciation to Matthew Reichert, Dan Hall, and Alex Huffield at Montana State University (MSU) for their assistance in the early stage of this research.

Literature Cited

- (1). Hartt W. H.; Charvin, S.; Lee, S. K. *Influence of permeability reducing and corrosion inhibiting admixtures in concrete upon initiation of salt induced embedded metal corrosion*. Prepared for the Florida Department of Transportation. **1999**.

- (2). Martín-Pérez, B.; Zibara, H.; Hooton, R.D.; Thomas, M.D.A. A study of the effect of chloride binding on service life predictions. *Cement. Concrete. Res.* **2000**, 30, 1215.
- (3). Samples L. M.; Ramirez, J. A. *Methods of corrosion protection and durability of concrete bridge decks reinforced with epoxy-coated bars, Phases I.* FHWA/IN/JTRP-98/15. Purdue University, IN. **1999**.
- (4). Page, C. L.; Ngala, V.T.; Page, M.M. Corrosion inhibitors in concrete repair systems. *Mag. Concrete. Res.* **2000**, 52, 25.
- (5). Glass, G. K.; Buenfeld, N. R. Chloride-induced corrosion of steel in concrete. *Progr. Struct. Eng. Mater.* **2000**, 2, 448.
- (6). Al-Otoom, A.; Al-Khlaifa, A.; Shawaqfeh A. Crystallization technology for reducing water permeability into concrete. *Ind. Eng. Chem. Res.* **2007**, 46, 5463
- (7). Cady, P.D.; Weyers, R.E. Predicting service life of concrete bridge decks subject to reinforcement corrosion. Corrosion forms and control for infrastructure. *ASTM Spec. Tech. Publication* **1992**, 1137, 328.
- (8). Liam, K.C.; Roy, S.K.; Northwood, D.O. Chloride ingress measurements and corrosion potential mapping of a 24 Year old reinforced concrete jetty structure in a tropic marine environment. *Mag. Concrete Res.* **1992**, 44, 205.
- (9). Hartt, W.; Nam, J. *Critical parameters for Corrosion Induced Deterioration of Marine Bridge Substructures in Florida.* Prepared for the Florida Department of Transportation. **2004**.
- (10). Berke N. S.; Weil T. G. *World wide review of corrosion inhibitors in concrete. Advances in concrete technology*; CANMET: Ottawa, **1994**.

- (11). Ramachandran, V. S. *Concrete admixtures handbook: properties, science, and technology*; 2nd ed. Noyes Publications: Park Ridge, NJ, USA; **1995**.
- (12). Lane, D. R.; Melendez, J. A.; Munteanu, V. F.; Kinney, F. D. Corrosion inhibiting admixture for concrete. *US Patent* **2002**, 6,340,438.
- (13). V.S. Sastri. *Corrosion inhibitors: principles and applications*, Willey: England, 1998.
- (14). Hansson, C. M.; Mammolite, L.; Hope, B. B. Corrosion inhibitors in concrete – Part I: The principles. *Cement. Concrete. Res.* **1998**, 28, 1775.
- (15). Monticelli, C.; Frignani, A.; Trabanelli, G. A. Study on corrosion inhibitors for concrete application. *Cement Concrete Res.* **2000**, 30, 635.
- (16). Morris, W.; Vázquez, M. A. Migrating corrosion inhibitor evaluated in concrete containing various contents of admixed chlorides. *Cement. Concrete. Res.* **2002**, 32,259.
- (17). Munteanu V. F.; Kinney F. D. *Corrosion inhibition properties of a complex inhibitor - mechanism of inhibition*; CANMET; Ottawa. **2000**.
- (18). Gaidis J. M. Chemistry of corrosion inhibitors. *Cement Concrete Comp.* **2004**, 26, 181.
- (19). Rosenberg, A. M.; Gaidis, J. M. The mechanism of nitrite inhibition of chloride attack on reinforcing steel in alkaline aqueous environments. *Mater. Performance.* **1979**, 18, 45.
- (20). Tritthart, J.; Banfill, P. F. G. Nitrite binding in cement. *Cement. Concrete. Res.* **2001**, 31, 1093.
- (21). Craig, R. J.; Wood, L. E. Effectiveness of corrosion inhibitors and their influence on the physical properties of Portland cement mortars. *Highway Res. Rec.* **1970**, 328,77

- (22). Gonzalez, J. A.; Ramirez, E.; Bautista, A. Protection of steel embedded in chloride containing concrete by means of inhibitors. *Cement. Concrete. Res.* **1998**, 28, 577.
- (23). Nmai, C. K.; Farrington, S. A.; Bobrowski, G. S. Organic-based corrosion-inhibiting admixture for reinforced concrete. *Concrete Intl.* **1992**, 14, 45.
- (24). Campbell, S.; Jovancicevic, V. Corrosion inhibitor film formation studied by ATR-FTIR. *CORROSION 99*; San Antonio, TX; USA. Paper No.484, 1999.
- (25). Nmai, C.K. Multi-functional organic corrosion inhibitor. *Cement. Concrete. Comp.* **2004**, 26(3),199.
- (26). Nguyen, T. A.; Shi, X. Corrosion and inhibition performances at the steel-mortar interface. Part 2: An electrochemical characterization. *Ind. Eng. Chem. Res.*, under review.
- (27). Sarkar, S. L.; X, A. Preliminary study of very early hydration of superplasticized C₃A+Gypsum by environmental SEM. *Cement. Concrete. Res.* **1992**, 22, 605.
- (28). Swift, A.; Paul, A. J.; Vickerman, J. C. Investigation of the surface activity of corrosion inhibitors by XPS and time-of-flight SIMS. *Surf. Interface Anal.* **1993**, 20(1), 27.
- (29). Marcotte, T. D.; Hansson, C. M. The effect of the electrochemical chloride extraction treatment on steel-reinforced mortar. Part II: Microstructural characterization. *Cement. Concrete. Res.* **1999**, 29, 1561.
- (30). Beaudoin, J. J.; Ramachandran, V. S. *Handbook of analytical techniques in concrete science and technology: Principles, techniques, and applications*; William Andrew Publishing: Norwich, NY, **2001**.

- (31). Pratt, P. L.; Ghose, A. Electron microscopy studies of Portland cement microstructures during setting and hardening. *Phil. Trans. R. Soc. Lond. A* **1983**, 310, 93.
- (32). Briggs, D; Grant, J. T, *Surface analysis by Auger and X-ray photoelectron spectroscopy*; IM publications and Surface Spectra Ltd.: Chichester, **2003**.
- (33). Berke, N. S.; Sundberg, K. M. The effects of calcium nitrite and microsilica admixtures on corrosion resistance of steel in concrete. Proceedings of Paul Klieger Symposium on Performance of Concrete. ACI SP-122. **1990**, 269
- (34). Bertolini L., B.; Elsener, P. P.; Polder, R. *Corrosion of Steel in Concrete: Prevention, Diagnosis, Repair*. Wiley-VCH, Verlag GmbH & Co.: KgaA, Weinheim, **2004**.
- (35). Famy, C.; Brough, A. R.; Taylor, H. F. W. The C-S-H gel of Portland cement mortars: Part I. The interpretation of energy-dispersive X-ray microanalyses from scanning electron microscopy, with some observations on C-S-H, AFm and AFt phases compositions. *Cement. Concrete. Res.* **2003**, 33, 1389.
- (36). Chen, J. J.; Thomas, J. J.; Taylor; Hal F. W.; Jennings, H. M. Solubility and structure of calcium silicate hydrates. *Cement. Concrete. Res.* **2004**, 34, 1499.
- (37). Mindess, S.; Young, J. F. *Concrete*; Prentice-Hall: Englewood Cliffs, NJ, **1981**.
- (38). Richardson, I. G.; Groves, G. W., Microstructure and microanalysis of hardened ordinary Portland cement pastes. *J. Mater. Sci.* **1993**, 28,265.
- (39). Koleva, D. A.; Hu, J.; Fraaij, A. L. A.; Stroeven, P.; Boshkov, N; de Wit, J. H. W. Quantitative characterisation of steel/cement paste interface microstructure and corrosion phenomena in mortars suffering from chloride attack. *Corros. Sci.* **2006**, 48, 4001.

List of Figures and Tables

Figure 1. Representative morphology and microstructure from the fracture surface of mortars after 60 days of ponding by 3% NaCl solution, at the steel-mortar interfacial region: A) without salt or inhibitor admixed; B) with 3% NaCl admixed; C) with 3.8% NaCl admixed; D) with 3% NaCl and 0.05 M DGP admixed; E) with 3% NaCl and 0.5 M SN admixed; F) with 0.05 M DMEA and 3% NaCl admixed. All FESEM images were taken at magnification level of approximately 500 times.

Figure 2. Representative C/Ca signal ratios (a) and relative Cl content (b) of the fracture surface on the steel plate of samples after 60 days of ponding by 3% NaCl solution. The three characteristic peaks used were C 1s, Ca 2p and Cl 2p at binding energy of approximately 290eV, 345eV, and 200eV respectively. The average and standard deviation were calculated using XPS data from three different sites on each sample.

Figure 3. Evolution of Cl/Ca (a) and N/Ca (b) elemental ratios of the fracture surface on various mortar samples during the 180-day ponding by 3% NaCl solution. The data were averaged for EDX measurements taken from three rusty sites and three non-rusty sites respectively on each sample. PCM stands for Portland cement mortar.

Figure 4. Na/Ca (a), C/Ca (b), Al/Ca (c), S/Al (d), and Si/Ca (e) elemental ratios of the fracture surface on various mortar samples over the 180-day ponding by 3% NaCl solution, with data averaged for EDX measurements taken at day 0, day 60 and day 180.

Table 1. Chemical composition of Type I/II low-alkali Portland cement

Table 2. Physical properties of Type I/II low-alkali Portland cement

Table 3. Mix design of mortar samples investigated (percentages and concentrations were by weight of water)

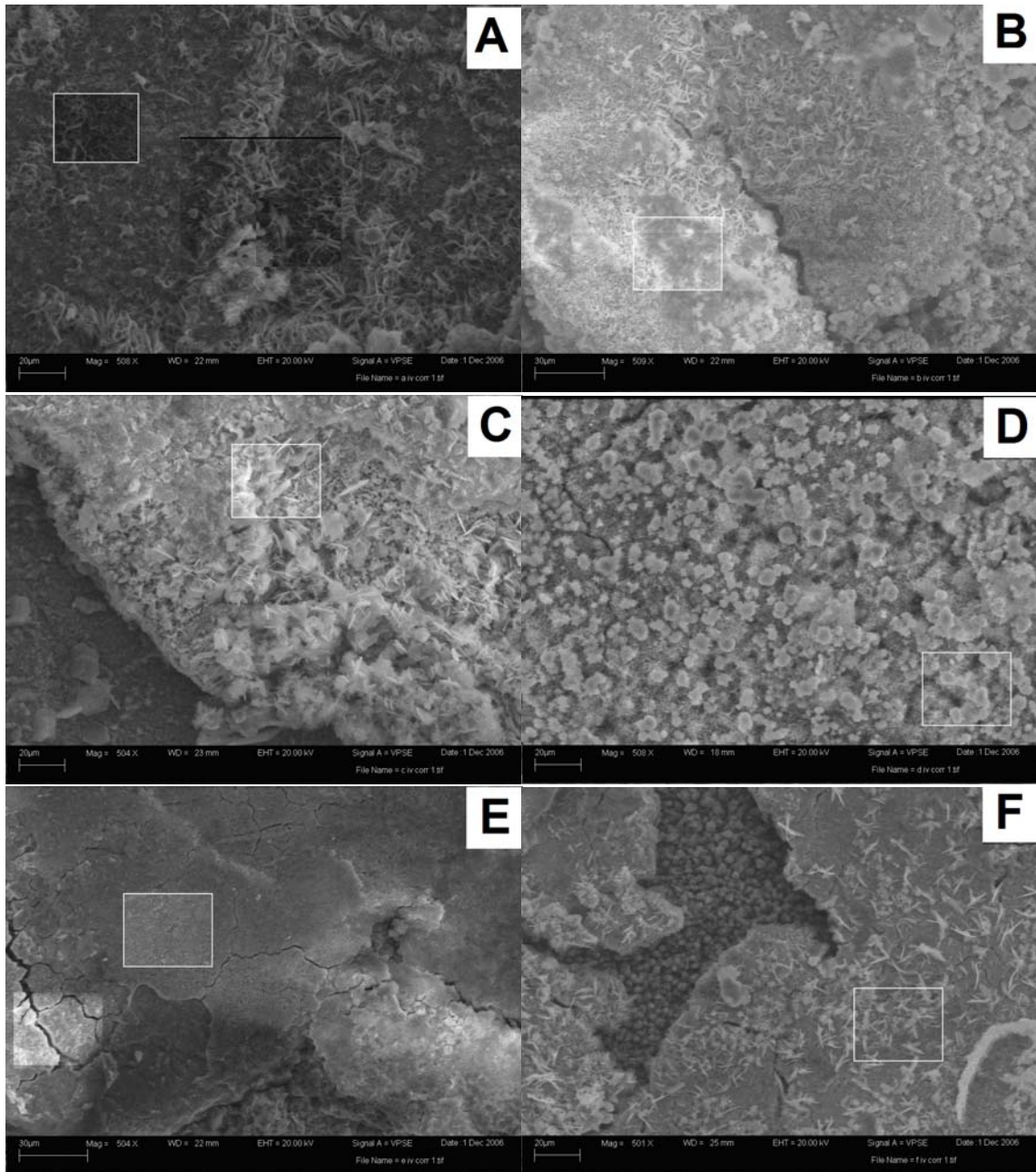
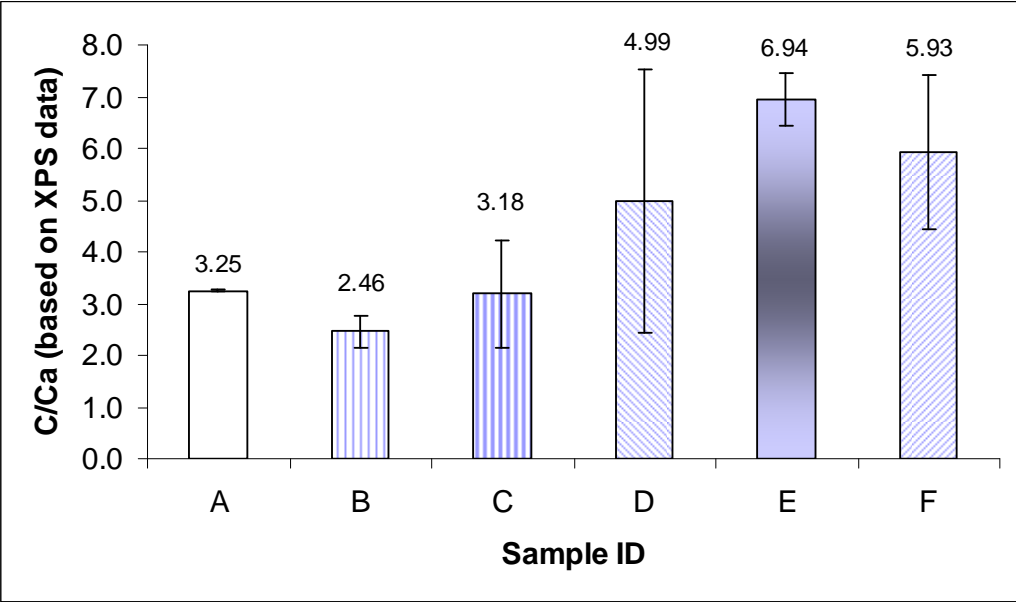
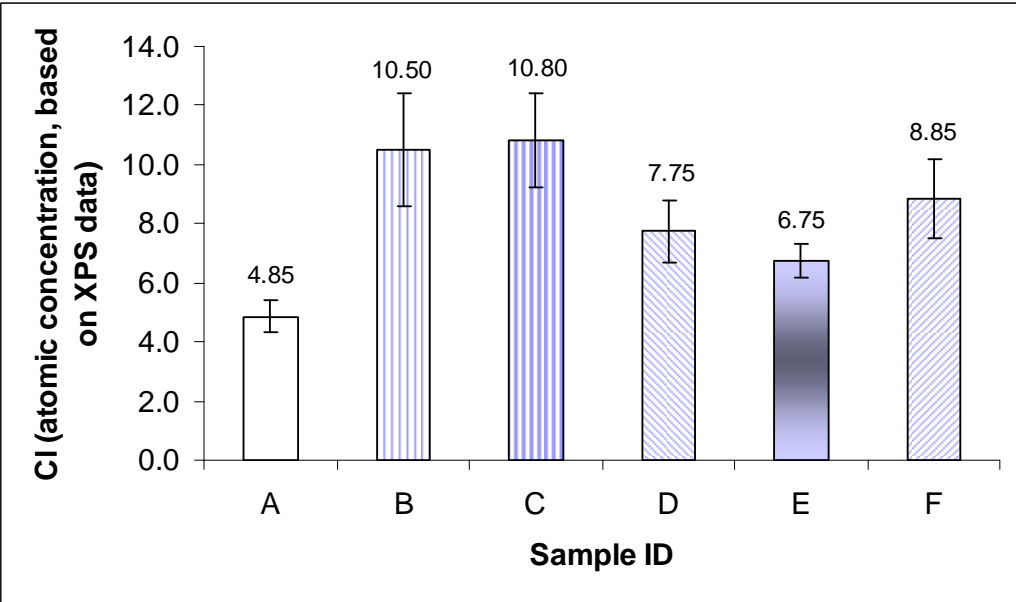


Figure 1.

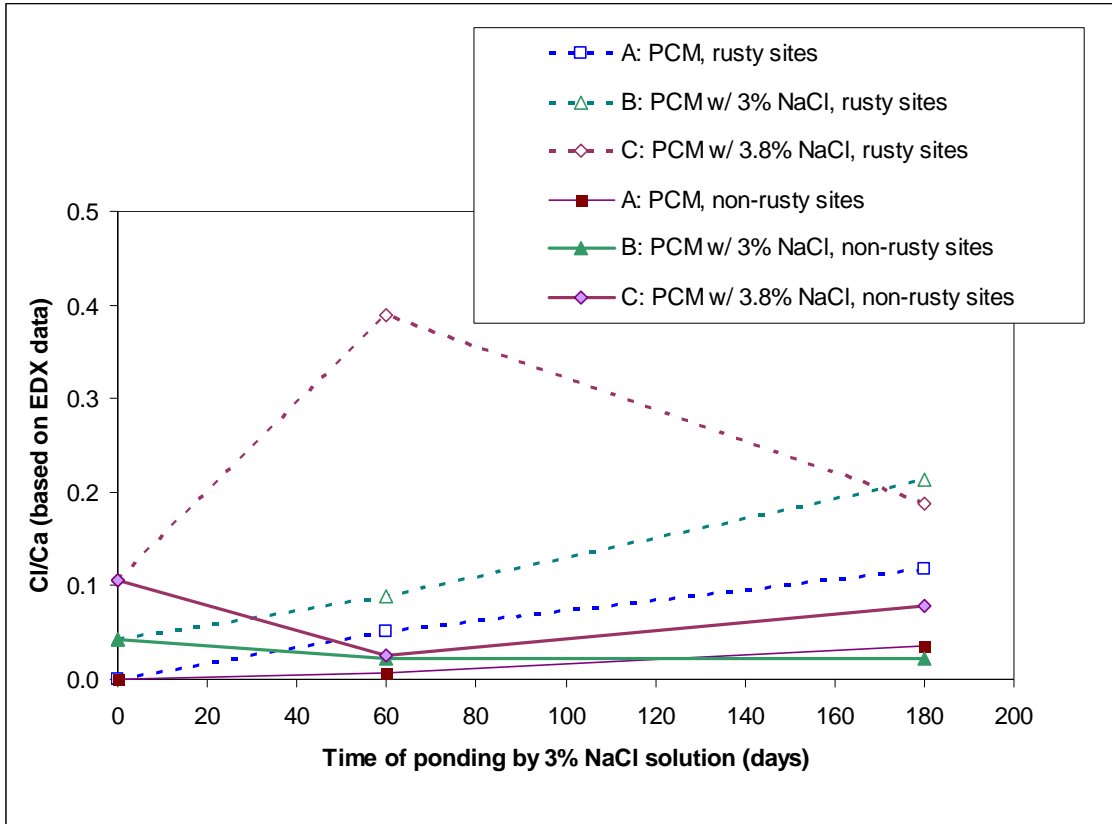


(a)

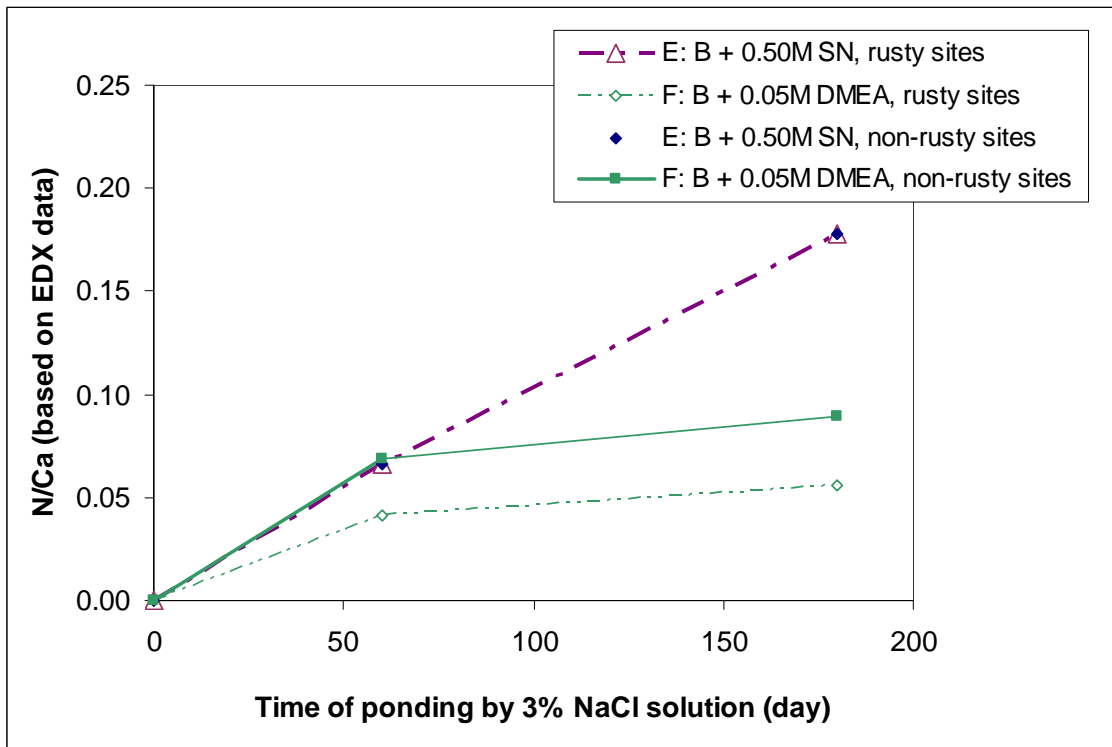


(b)

Figure 2.

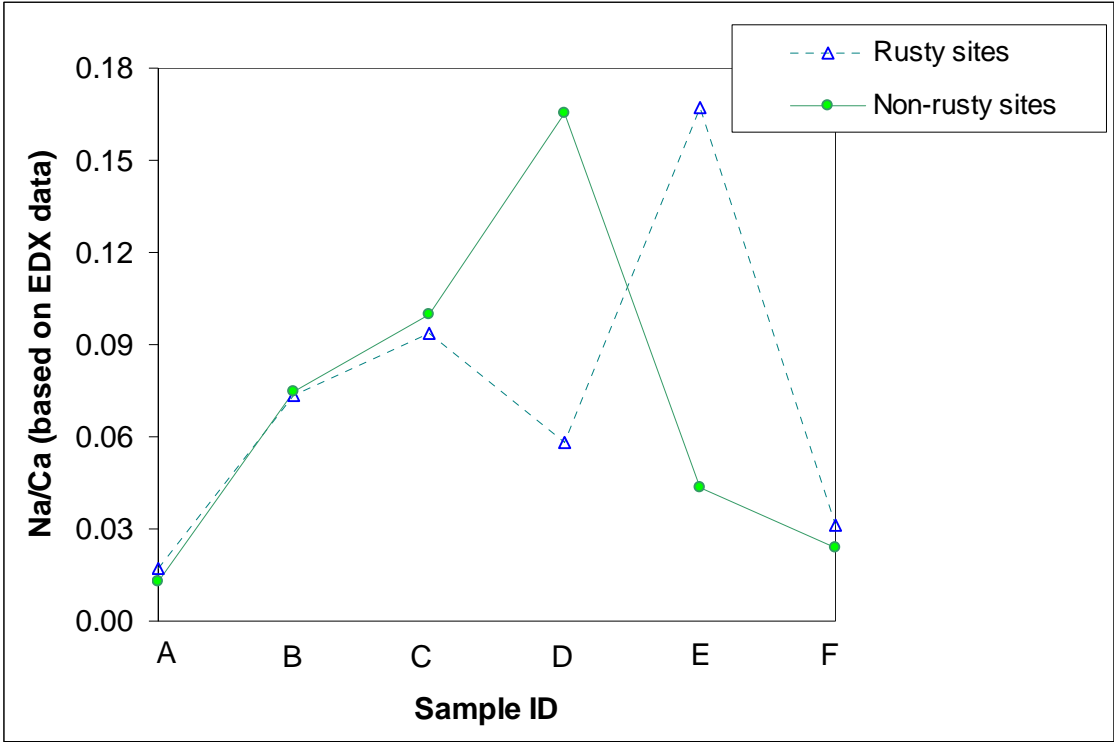


(a)

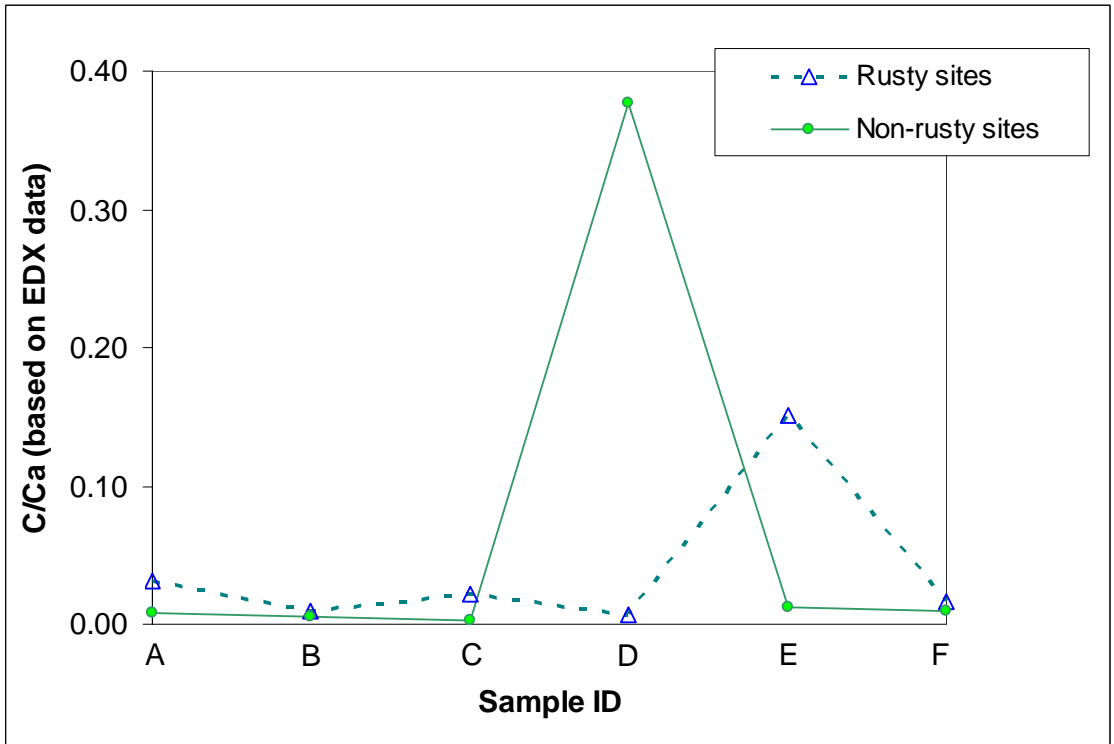


(b)

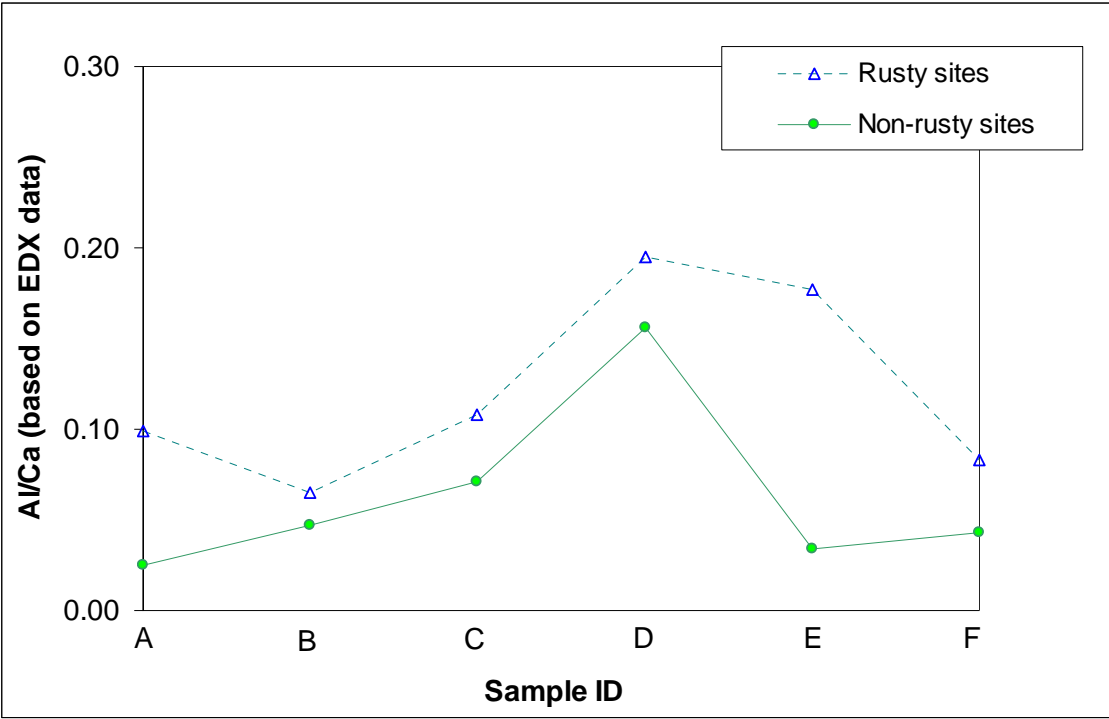
Figure 3.



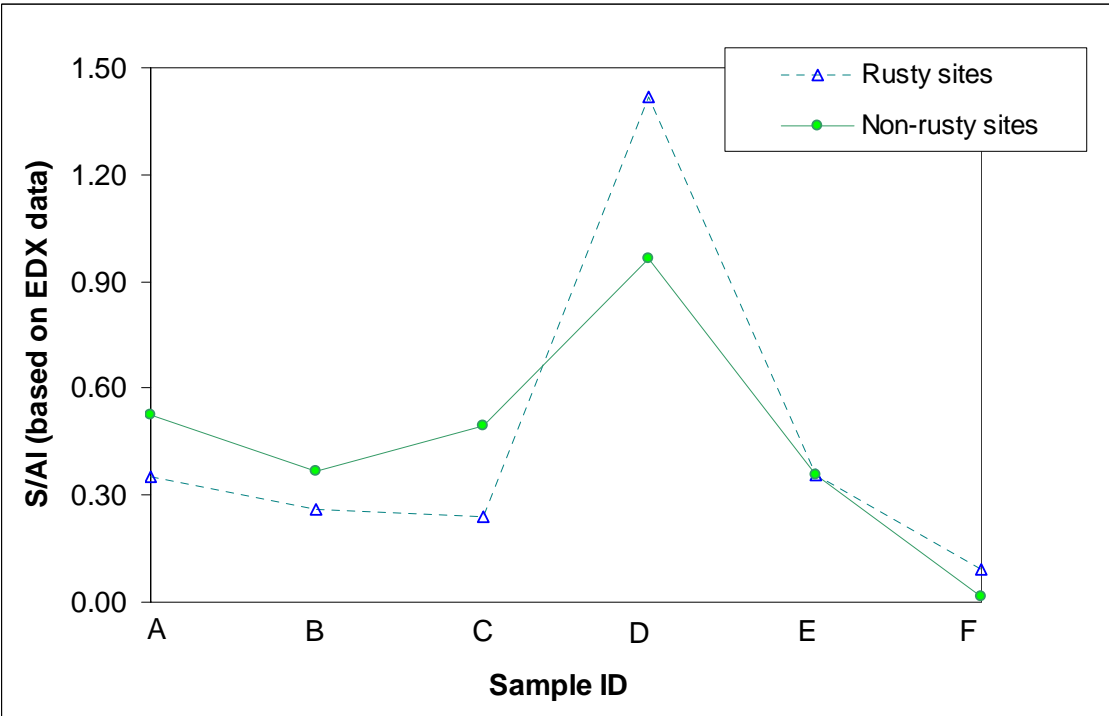
(a)



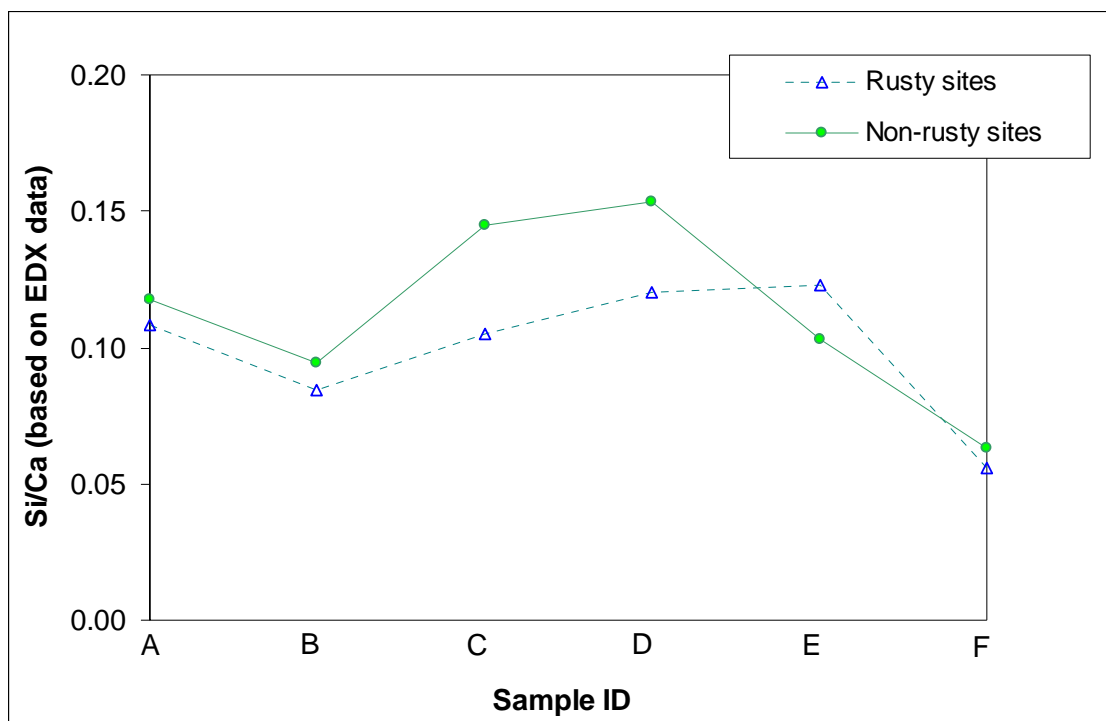
(b)



(c)



(d)



(e)

Figure 4.

Table 1.

Item	Spec. Limit	Test Result
SiO ₂ (%)	N/A	20.4
Al ₂ O ₃ (%)	6.0 max	3.7
Fe ₂ O ₃ (%)	6.0 max	3.2
CaO (%)	N/A	63.3
MgO (%)	5.0 max	3.2
SO ₃ (%)	3.0 max	2.6
Loss on Ignition (%)	3.0 max	2.7
Na ₂ O (%)	N/A	0.1
K ₂ O (%)	N/A	0.4
Insoluble Residue (%)	0.75 max	0.43
CO ₂ (%)	N/A	1.7
Limestone (%)	5.0 max	4.0
CaCO ₃ in Limestone (%)	70 min	98
Tot. Alkalies (% as Na ₂ O)	0.60 max	0.37
Potential Compound Composition (%)		
C ₃ S	N/A	56
C ₂ S	N/A	16
C ₃ A	8.0 max	4.5
C ₄ AF	N/A	10
C ₄ AF+2(C ₃ A)	N/A	19
C ₃ S+4.75(C ₃ A)	100 max	78

Table 2.

Item	Test Method (ASTM)	Spec. Limit	Test Result
Air content of mortar,%	C185	12.0 max	7.9
Blaine Fineness,m ² /Kg Air	C204	280 min	397
permeability test		420 max	
Autoclave Expansion,%	C151	0.80 max	0.03
Normal Consistency,%	C187	N/A	26.6
Compressive strengths, psi(MPa)	C109		
1-Day		N/A	1998(13.8)
3-Day		1740(12.0)min	3472(23.9)
7-Day		2760(19.0)min	4600(31.7)
Setting Times, minutes	C191		
Vicat Initial		45 min	111
Vicat Final		375 max	240
Pass 325 mesh,%		72 min	98.7
Heat of hydration (cal/g)-7days		N/A	70.7
False set, %	C451	50 min	85

Table 3.

Samples	A	B	C	D	E	F
Cement	×	×	×	×	×	×
Sand	×	×	×	×	×	×
Water	×	×	×	×	×	×
3% NaCl		×		×	×	×
3.8% NaCl			×			
0.05M DGP				×		
0.5M SN					×	
0.05M DMEA						×

**Corrosion and Inhibition Performances at the Steel-Mortar
Interface. Part 2: An Electrochemical Characterization**

Tuan Anh Nguyen¹ and Xianming Shi^{1,2,*}

¹ *Corrosion and Sustainable Infrastructure Laboratory, Western Transportation Institute, PO
Box 174250, College of Engineering, Montana State University, Bozeman, MT 59717-4250,
USA*

² *Civil Engineering Department, 205 Cobleigh Hall, Montana State University,
Bozeman, MT 59717-2220, USA*

* *Corresponding Author; Phone: 1-406-994-6486; Fax: 1-406-994-1697; E-mail:
Xianming_s@coe.montana.edu*

Abstract

This research aimed to unravel the role of salt contamination and admixed corrosion inhibitors in the processes of cement hydration and rebar corrosion, using mostly electrochemical impedance spectroscopy. The admixing of all three inhibitors in fresh mortar was found to increase the polarization resistance of steel, indicating reduced corrosion rate of the steel over 48-day exposures to salt ponding. 0.05M N,N'-dimethylethanolamine was the most capable and reliable corrosion inhibitor, followed by 0.5M sodium nitrite; whereas 0.05M disodium β -glycerophosphate was a slower and less capable corrosion inhibitor. The admixing of NaCl and inhibitors in fresh mortar generally increased and decreased the electrical resistance of hardened mortar, respectively. The admixing of inhibitors in fresh mortar consistently increased the capacitance of hardened mortar. The effect of sodium nitrite on the resistance of steel-mortar interfacial film offset that of NaCl, attributable to the formation of a protective ferric oxide film.

1. Introduction

For highway bridges and other reinforced concrete structures, the corrosion of reinforcing steel in concrete has been a major durability problem with serious economic and safety implications ¹. There is consensus that the most effective means to address this problem can be achieved at the design stage by using adequate concrete cover and high-quality concrete. Other practices at this stage include: the addition of corrosion inhibitors or permeability-reducing admixtures to fresh concrete; the surface treatment of steel rebar; or the use of alternative reinforcement materials.

The use of corrosion inhibitors for new structures, also known as corrosion inhibiting admixtures (CIAs), seems to be a promising solution in controlling rebar corrosion in concrete ²⁻⁶, by changing the local environment at the steel-concrete interface. In a recent laboratory study ⁷, however, while both calcium-nitrite-based and organic CIAs delayed the onset of corrosion, their effect on the corrosion rate of the embedded steel was found to be insignificant once active corrosion had been initiated. While nitrite-based CIAs have been reported to alter the strength properties of hardened concrete or change the curing behavior of fresh concrete ⁴, there is little research on the effect of admixed inhibitors or chlorides on the microstructure and chemistry of hardened concrete. Therefore, more research is needed to help understand the role of salt contamination and CIAs in the processes of cement hydration and rebar corrosion.

In this work, three CIAs, sodium nitrite [SN, NaNO_2], disodium β -glycerophosphate [DGP, $\text{C}_3\text{H}_7\text{Na}_2\text{O}_6\text{P}$] and N,N'-dimethylethanolamine [DMEA, $(\text{CH}_3)_2\text{NCH}_2\text{CH}_2\text{OH}$] were investigated. Inorganic CIAs such as nitrites have been considered very effective, since they act as a passivating agent with oxidizing properties to inhibit the anodic reaction of corrosion process. Nonetheless, there are concerns over the performance of such inhibitors when used in low dosage or where cracks in the concrete allow leaching to occur. The consensus is that

a sufficiently high nitrite/chloride molar ratio needs to be established and maintained for effective inhibition. One study estimated the critical nitrite/chloride ratio for calcium nitrite to be about 0.6 in order to prevent the onset of corrosion⁸. SN was found to be a more effective corrosion inhibitor than potassium chromate and sodium benzoate, but had some detrimental effect on concrete strength⁹. Organic CIAs act by adsorption on the metal surface, forming a layer that may inhibit both the anodic and cathodic reactions of corrosion process. Laboratory tests, in aqueous solution or in concrete, have shown conflicting results about the efficiency and the minimum concentration required of organic CIAs for effective inhibition^{7, 10-11}. There are also limited data on the long-term efficiency of organic inhibitors¹². Monticelli et al. (1995) reported that the corrosion resistance of steel rods embedded in a chloride-polluted mortar was excellent in the presence of SN alone as well as in the presence of a low-concentration DGP-SN admixture¹³. SN was believed to allow the surface oxide to form and repair on defects while DGP was known to protect the passive conditions by chemisorption on the oxide film, and there was synergetic inhibition action between the two. Monticelli et al. (2000) reported that over 30-day exposures, 0.05M SN and 0.05M DGP were both able to prevent pitting corrosion of steel in a saturated calcium hydroxide solution containing 0.1 M chloride ions¹⁴. Data from Fourier transform infrared spectroscopy and cyclic voltammetry further confirmed that DGP interacted with the steel surface by quick chemisorption and both SN and DGP formed an impervious surface film on steel to block any localized corrosion attack¹⁵. Welle et al. (1997) reported that DMEA chemisorbed from aqueous solution onto the oxidized steel surface, displaced chloride ions from the steel surface, and formed a durable passivating film¹⁶.

In this paper (Part 2), we report on using electrochemical impedance spectroscopy (EIS) to characterize the behavior of steel-mortar samples admixed with sodium chloride and corrosion inhibitors. In a separate paper (Part 1), we report on using field emission scanning

electron microscopy/ energy dispersive x-ray spectroscopy and X-ray photoelectron spectroscopy to unravel the role of salt contamination and admixed corrosion inhibitors in the processes of cement hydration and rebar corrosion ¹⁷. EIS provides information on interfaces and thus shed light on the active-passive behavior and properties of the metal oxide formed on the steel surface. It has also been used to study the migration behavior of the inhibitor ions towards the reinforcing steel surface ^{10, 11, 18}; and to study the change of electrical resistance of bulk concrete as well as corrosion rate of rebar in concrete due to the admixing of corrosion inhibitors ⁷.

2. Experimental procedures

2.1. Materials. An ASTM specification C150-07 Type I/II low-alkali Portland cement (ASH Grove Cement Company Clancy, MT) was used in this study. The chemical composition and physical properties of the cement are reported elsewhere ¹⁷. The fine aggregates used were river sand sifted with a 250 μm sieve before proportioning and admixing. Steel plate (C4130 carbon steel) was purchased from Metal Samples, Inc. (Munford, AL). De-ionized water was used in the experiment.

2.2. Sample preparation. All the mortar samples were prepared with cement: sand: water mass ratio of 1: 0.075: 0.5. The percentages and concentrations of chloride and inhibitors added to the mortar were by weight of water. Table 1 shows the mix design for the six types of samples with various contents of admixed chloride and inhibitors. The chloride contamination levels (3% and 3.8% by weight of water) in fresh mortar were used to simulate the scenarios where seawater is used for concrete mixing and construction for seashore structures and components. The steel plate was cleaned with de-ionized water and acetone and dried in advance. For each sample, fresh mortar was poured into a plastic tube (2.2cm² of surface area, 5mm deep) attached to a square steel plate (2.5cm \times 2.5cm) using epoxy resin

and carefully compacted to minimize air voids. Following curing in a wet chamber for 28 days at approximately 20°C and 95% relative humidity, each steel-mortar sample was demoulded from the plastic tube and another plastic tube (2.2cm² of surface area, 10mm deep) was sealed on top of it to serve as a reservoir. To initiate steel corrosion, all samples were then ponded with 3% NaCl solution. Three specimens were prepared for each mix design to validate the reliability of test results.

2.3. Electrochemical measurements. For each mortar sample, a platinum mesh was placed in the pond as the counter electrode and a saturated calomel electrode (SCE) was used as the reference electrode. Over the 48-day salt ponding period, a Gamry Electrochemical Multiplexer ECM8 was used to monitor the open circuit potential (OCP) of square steel plates attached to mortar and to measure the EIS data. EIS measurements were taken periodically by polarizing the steel at ± 10 mV around its OCP and with a frequency between 300 KHz and 5 mHz (10 points per decade). The Gamry analysis software was used to plot and fit the EIS data.

It should be noted that the OCP data measured were affected by both the steel corrosion and the electrical resistance of hardened mortar, as the working electrode (the steel) was separated from the reference electrode (the SCE in the pond) by the 5-mm thick mortar.

3. Results and discussion

Figures 1-4 show the Nyquist diagrams for these six steel-mortar samples, respectively, at the salt ponding time of 1 day, 9 days, 22 days, and 43 days. For most of the mortar samples, the equivalent circuit with three time constants and a diffusion element (also used by Song, 1998¹⁹) as shown in Figure 5 was found to provide the best fit to the EIS data.

For some of the mortar samples, such as the control (A: without any salt or inhibitor admixed), their EIS data showed a different pattern than the ones with salt admixed and

would fit well using a simpler equivalent circuit with two time constants (without the intermediate frequency loop characterizing the corrosion products). In order to compare the evolution of circuit parameters (R and C) over the salt ponding period, however, we consistently used the same equivalent circuit in Figure 5 for analyzing all the EIS data. As such, we divide the electrochemical system into three integrated interfaces: electrolyte-bulk mortar interface; steel-mortar interface and steel-electrolyte interface. Even though the mortar contains a certain electrolyte due to its porosity, the steel-mortar and the steel-electrolyte interface are different in terms of which material is in direct contact with the steel. The Warburg diffusion impedance (W) associated with oxygen transport was assumed to be similar for all the samples, i.e., $1 \times 10^{-18} \text{ S.s}^{1/2}$, for the best fitting procedure.

It is interesting to note that samples A and E had similar EIS patterns, both of which were different than those for other samples. At low frequency range both the control (sample A, see Figure 1) and the sample E (with 3% NaCl and 0.5M SN admixed, see Figure 3) featured a higher resistance corresponding to a stronger barrier effect, whereas in other samples the diffusion process had dominated.

The EIS data indicated that the fitting coefficients for C_1 (capacitance of steel-mortar interface) and C_2 (capacitance of steel-electrolyte interface) were generally in the range of 0.3-0.9 (with 1 being the perfect fit), indicating that those capacitances were not perfect, attributable to the heterogeneous interfacial conditions and the competing processes (e.g., inhibitor absorption vs. chloride attack, steel passivation vs. pitting) occurring at the steel surface.

3.1. The electrolyte-bulk mortar interface. In the Nyquist diagrams, the high frequency loop can be attributed to the properties of the electrolyte-bulk mortar interface, with R_0 and C_0 representing the electrical resistance and capacitance of the bulk mortar mix. These two parameters have very important practical implications, as they can affect the rate of steel

corrosion propagation in concrete, the efficiency of electrochemical rehabilitation of reinforced concrete, and the electrical properties of concrete in general.

Figure 6 shows the evolution of R_0 and C_0 over time for the steel-mortar samples under salt ponding. Differences in the initial value of mortar resistance (R_0) were derived from the differences in microstructure and chemistry (especially cement hydrates) of the six 28-day old mortar samples. Over the 48 days of salt ponding, the evolution of R_0 and C_0 over time and their differences between samples can be accounted for by the ever-changing pore fluid chemistry and the continued cement hydration with active participation of chloride or inhibitors.

The admixing of NaCl in fresh mortar generally increased the electrical resistance of hardened mortar, especially in the first month of salt ponding (see Figure 6a). Note that to examine the influence of salt contamination in fresh mortar, the data from the early stage of ponding by 3% NaCl solution are more elucidatory as they were not as clouded by the chloride ingress as the data from the later stage. In the first three weeks, for the non-inhibited mortars (samples A, B and C), the mortar resistance increased significantly over time, which may be attributed to the continued cement hydration resulting in denser mortar microstructure and reduced porosity. The mortar resistance then fluctuated, indicating possibly another competing mechanism at work. As the ponding progressed, the mortar matrix became more conductive with the increase in moisture and salt content, which would tend to reduce mortar resistance.

The admixing of corrosion inhibitors in fresh mortar generally decreased the electrical resistance of hardened mortar (see Figure 6a), which is not beneficial in terms of controlling the rate of rebar corrosion propagation. For the mortar admixed with 0.5M SN (sample E), however, the mortar resistance increased significantly with time of salt ponding, eventually exceeding that of two non-inhibited mortars (samples A and B). For sample E, this along

with the significant increase of C_0 with time of salt ponding may be explained by the modification of the mortar microstructure by SN. For the mortars admixed with 0.05M DGP (sample D) or 0.05M DMEA (sample F), their electrical resistance was consistently lower than that of the non-inhibited mortars and relatively stable over time. As such, DGP and DMEA are unlikely to be inhibitors that would block the mortar pores and thus reduce the cathodic current of steel corrosion by limiting the ingress of oxygen, whereas SN seems to have such function.

As shown in Figure 6b, the admixing of corrosion inhibitors in fresh mortar consistently increased the capacitance of hardened mortar (samples D, E, and F, compared with sample B). This may be attributed to the increased dielectric constant of mortar matrix as well as the altered mortar microstructure and cement hydrates in the presence of the inhibitors. The capacitance value C_0 obtained from all four diagrams are in range of 1-10 nF.cm⁻² for the first 30 days of salt ponding. This order of magnitude is much lower than data reported for bulk concrete (1-10 μF.cm⁻²)¹¹, but similar to data reported for bulk mortar (~0.8 nF.cm⁻²)²⁰. Compared with concrete samples, the use of much smaller sand (maximum size of 250 μm) in this study along with a very small sand-to-cement weight ratio (0.075, no other aggregates) led to much denser microstructure of the mortar samples, which can account for the much lower values in electrical capacitance.

3.2. The steel-mortar interface. In the Nyquist diagrams, the intermediate frequency loop can be attributed to the properties of the steel-mortar interface, with R_1 and C_1 representing the electrical resistance and capacitance of the interfacial film consisting of mainly the corrosion products. Figures 7a, 7b and 7c show the evolution of R_1 and C_1 over time for some of the steel-mortar samples under salt ponding, respectively. According to Dhouibi et al. (2002), differences in the initial value of resistance R_1 were derived from the differences in ionic resistance of this interfacial film¹¹.

As shown in Figure 7a, the admixing of NaCl in fresh mortar significantly decreased the resistance of the steel-mortar interfacial film, indicating a more conductive interface due to the presence of NaCl and corrosion products. For the mortar admixed with 3% NaCl (sample B), R_1 increased with time, attributable to the formation of corrosion products at the interface, likely iron oxides and oxychloride complexes¹⁰⁻¹¹. For the Portland cement mortar without any admixed salt (sample A), R_1 decreased significantly after approximately 30 days of ponding by 3% NaCl, signifying that the chloride solution had reached the steel-mortar interface. For the mortar admixed with 3% NaCl and 0.5M SN (sample E), it is interesting to note that the evolution of its R_1 followed a pattern similar to sample A, indicating that the effect of sodium nitrite on the resistance of steel-mortar interfacial film offset that of NaCl.

As shown in Figure 7b, after approximately 30 days of salt ponding, all three inhibited mortar samples (D, E, F) had lower R_1 values than the non-inhibited mortar (B), implying different amounts and characteristics of corrosion products at the steel-mortar interface. As shown in Figure 7c, the admixing of NaCl in fresh mortar generally increased the capacitance of the steel-mortar interfacial film, showing that the admixed salt changed the dielectric properties of the interface layer, likely through the formation of corrosion products.

3.3. The steel-electrolyte interface. In the Nyquist diagrams, the low frequency loop can be attributed to the properties of the steel/electrolyte interface, with R_2 and C_2 representing the charge transfer resistance of steel (mainly polarization resistance) and the capacitance of double layer and inhibitor film on the steel surface, as well as the Warburg impedance W characterizing the diffusion of species through the interface.

Figure 8 shows the corrosion current density (i_{corr}) of steel as a function of mix design and salt ponding time, where the upper bars ($i_{\text{corr}} > 1 \mu\text{A}/\text{cm}^2$) indicate very active corrosion

state of steel according to literature²¹. i_{corr} was calculated as B/R_2 , with $B = 52 \text{ mV}$ for passive state of steel (when $i_{\text{corr}} < 0.1 \mu\text{A}/\text{cm}^2$) or 25mV if otherwise.

As shown in Figure 8, the steel plates attached to the 5-mm thick non-inhibited mortar samples (A, B and C) had very active corrosion since the early days of salt ponding by 3% NaCl solution. The samples studied featured a very aggressive environment for the steel, since the mortar had a high water-to-cement ratio (0.5), was admixed with high concentrations of chloride (except sample A), and then ponded by 3% NaCl solution. The admixing of NaCl in fresh mortar generally reduced the open circuit potential (OCP) of the steel, especially in the first month (samples B and C vs. sample A, see Figure 9a), attributable to exacerbated steel corrosion and increased electrical resistance of hardened mortar.

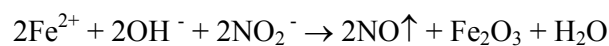
The admixing of all three inhibitors in fresh mortar was found to increase the polarization resistance of steel, indicating reduced corrosion rate of the steel over 48-day exposures to salt ponding. The evolution of i_{corr} over time of salt ponding indicates that 0.05M DMEA (sample F vs. sample B) was the most capable and reliable corrosion inhibitor, followed by 0.5M SN (sample E vs. sample B); whereas 0.05M DGP (sample D vs. sample B) was a slower and less capable corrosion inhibitor.

3.4. Inhibition mechanisms

3.4.1. N,N'-dimethylethanolamine (DMEA). Figure 9b shows that the admixing of 0.05M DMEA in fresh mortar raised or reduced the OCP of the steel in a cyclic manner, when comparing sample B (with 3% NaCl admixed) and sample F (with 3% NaCl and 0.05M DMEA admixed). This confirms some of the inhibition mechanisms identified by a previous study in aqueous solutions¹⁶, suggesting that DMEA was able to displace chloride ions from the steel surface and to protect the surface passive film. The partial displacement of chloride ions accompanied by the chemisorption of DMEA is confirmed in our other paper (Part 1)¹⁷.

The passive film on the steel surface, however, was not durable over the 48-day salt ponding period. This differed from the finding from the study in aqueous solutions¹⁶, where the DMEA-to-chloride concentration ratio was much higher and a durable passivating film was formed by DMEA on the steel surface. As suggested by the corrosion current density data ($i_{\text{corr}} \sim 0.1 \mu\text{A}/\text{cm}^2$ over the 48-day salt ponding, see Figure 8), DMEA effectively delayed the onset of steel corrosion and inhibited the steel corrosion even when the passive film was compromised (e.g., when the OCP values dropped below $-0.6 \text{ V}_{\text{SCE}}$). The simultaneous reduction in the OCP and in the i_{corr} signified a “*cathodic inhibitor*” at work, i.e., the strong absorption of DMEA onto the steel surface inhibited the cathodic reaction of steel corrosion by limiting the access of oxygen to the steel⁴. The inhibition mechanisms of DMEA make it a very promising candidate for commercial corrosion inhibitor formulations, as it may offer synergistic benefits when used together with nitrites.

3.4.2. Sodium nitrite (SN). Based on the corrosion current density data (i_{corr}) shown in Figure 8, the steel in sample E (with 3% NaCl and 0.5M SN admixed) had very active corrosion until a few days into salt ponding, suggesting the mechanism that SN inhibits corrosion by reacting with ferrous ions to form a protective ferric oxide film. SN did not prevent the onset of steel corrosion, instead it significantly reduced the corrosion rate of the steel once active corrosion had been initiated, demonstrating its strong ability to repair defects. This differed from the findings from the study of calcium-nitrite-based and organic CIAs, where they were found to inhibit the initiation of chloride-induced corrosion but did not significantly affect the subsequent corrosion rates of steel⁷. Figure 9b shows that the admixing of 0.5M SN in fresh mortar raised the OCP of the steel, when comparing sample B (with 3% NaCl admixed) and sample E. This confirms that SN can serve as an “*anodic inhibitor*” to inhibit the anodic reaction of steel corrosion through passivation of the steel, as a result of the following reaction²:



This passivation mechanism accounted for the pattern similarity in the evolution of R_1 (electrical resistance of the steel-mortar interfacial film) over time between sample E and the control (A: without any salt or inhibitor admixed), as shown in Figure 7a. In other words, the effect of SN on R_1 offset that of NaCl, as they passivated and de-passivated the steel surface respectively. The formation of a protective film in the presence of 0.5M SN also accounted for the similarity in the EIS patterns between sample E and the control, as discussed earlier.

For sample E, the decay of the steel OCP over the 48-day salt ponding period (as shown in Figure 9b) coincided with the decrease of nitrite-to-chloride ratio over time. As the ponding progressed, the electrical resistance and capacitance of the mortar increased over time (see Figure 6); and eventually, the low i_{corr} values along with the diminished OCP enhancement signified a “*pore blocker*” at work, i.e., the modification of mortar matrix by SN blocked the pores critical to oxygen ingress and thus reduced the cathodic current⁴. The modification of mortar matrix by SN may account for its detrimental effect on concrete strength reported previously⁹. The inhibition mechanisms of SN make it a promising candidate for rehabilitating chloride-contaminated reinforced concrete where active corrosion of the embedded steel might have been initiated. In contrast, caution needs to be exercised when using SN as an inhibitor to be admixed in fresh concrete, considering its inability to prevent the onset of steel corrosion and its potential adverse impact on the concrete strength.

3.4.3. Disodium β -glycerophosphate (DGP). Based on the corrosion current density data (i_{corr}) shown in Figure 8, the steel in sample D (with 3% NaCl and 0.05M DGP admixed) had very active corrosion until 48 days into salt ponding. DGP did not prevent the onset of steel corrosion or bring the steel back to passive state ($i_{\text{corr}} < 0.1 \mu\text{A}/\text{cm}^2$ or so), whereas it constantly slowed down the pitting corrosion of the steel. This differed from the findings from a previous study of DGP, where the DGP-to-chloride concentration ratio was much

higher (0.5) and 0.05M DGP was able to prevent pitting corrosion of steel in a saturated calcium hydroxide solution containing 0.1 M chloride ions ¹⁴. Figure 9b shows that the admixing of 0.05M DGP in fresh mortar raised the OCP of the steel in the early stage of salt ponding, when comparing sample B (with 3% NaCl admixed) and sample D. This suggests that DGP was able to displace chloride ions from the steel surface and to protect the surface passive film. The partial displacement of chloride ions accompanied by the chemisorption of DGP is confirmed in our other paper (Part 1) ¹⁷. The passive film on the steel surface, however, was not durable over the 48-day salt ponding period. This differed from the finding from the study in aqueous solutions ¹⁵, where the DGP-to-chloride concentration ratio was much higher (0.5) and DGP formed an impervious surface film on steel to block any localized corrosion attack ¹⁵.

For sample D, the decay of the steel OCP over the 48-day salt ponding period (as shown in Figure 9b) coincided with the decrease of DGP-to-chloride ratio over time. As the ponding progressed, both the OCP and the i_{corr} values generally decreased. As discussed earlier, the evolution of mortar resistance ruled out the possibility of DGP being a “pore blocker”. Therefore, a reasonable hypothesis is that as the active corrosion propagated on the steel surface, the condition of the surface film formed by the chelating action of the phosphate group in DGP with the surface cations ¹⁵ improved, which was able to gradually slow down the steel pitting corrosion by limiting the ingress of oxygen. The inhibition mechanisms of DGP make it a not-so-ideal CIA in chloride-laden environments, but a promising candidate when used together with nitrites since the nitrites would offer better protection of the passive conditions of the steel surface while DGP can partially displace chloride ions and its chemisorption on the surface can inhibit the cathodic reaction of steel corrosion.

4. Conclusions

We used electrochemical tools (EIS and OCP) to characterize the behavior of steel-mortar samples admixed with sodium chloride and corrosion inhibitors. For most of the mortar samples, an equivalent circuit with three time constants and a diffusion element was found to provide the best fit to the EIS data. The admixing of NaCl and corrosion inhibitors in fresh mortar generally increased and decreased the electrical resistance of hardened mortar, respectively, especially in the early weeks of ponding by 3% NaCl solution. The admixing of corrosion inhibitors in fresh mortar consistently increased the capacitance of hardened mortar. The effect of sodium nitrite on the resistance of steel-mortar interfacial film offset that of NaCl, attributable to the formation of a protective ferric oxide film.

The admixing of all three inhibitors in fresh mortar increased the polarization resistance of steel in mortar, indicating reduced corrosion rate. 0.05M N,N'-dimethylethanolamine was the most capable and reliable corrosion inhibitor, followed by 0.5M sodium nitrite; whereas 0.05M disodium β -glycerophosphate was a slower and less capable corrosion inhibitor.

The inhibition mechanisms of DMEA (partial displacing of chloride ions and acting as *cathodic inhibitor*) make it a very promising candidate for commercial corrosion inhibitor formulations, as it may offer synergistic benefits when used together with nitrites. The inhibition mechanisms of SN (acting as *anodic inhibitor* and *pore blocker*) make it a promising candidate for rehabilitating chloride-contaminated reinforced concrete where active corrosion of the embedded steel might have been initiated. In contrast, caution needs to be exercised when using SN as an inhibitor to be admixed in fresh concrete, considering its inability to prevent the onset of steel corrosion and its potential adverse impact on the concrete strength. The inhibition mechanisms of DGP make it a not-so-ideal CIA in chloride-laden environments, but a promising candidate when used together with nitrites since the nitrites would offer better protection of the passive conditions of the steel surface while DGP can partially displace

chloride ions and its chemisorption on the surface can inhibit the cathodic reaction of steel corrosion.

Acknowledgements

This work was supported by the Research and Innovative Technology Administration under U.S. Department of Transportation through the University Transportation Center research grant. We would also like to extend our appreciation to Dr. Wei Chu, Matthew Reichert, Dan Hall, and Alex Huffield at Montana State University for their assistance in the early stage of this research.

Literature Cited

- (1) Glass, G. K.; Buenfield, N. R. Chloride induced corrosion of steel in concrete. *Prog. Struct. Engng. Mater.* **2000**, 2, 448-458.
- (2) Berke, N. S.; Sundberg, K. M. The effects of calcium nitrite and microsilica admixtures on corrosion resistance of steel in concrete. Proceedings of Paul Klieger Symposium on Performance of Concrete. ACI SP-122. **1990**, 269
- (3) Berke, N. S.; Weil, T. G. World wide review of corrosion inhibitors in concrete. *Advances in concrete technology*; CANMET: Ottawa, **1994**.
- (4) Hansson, C. M.; Mammolite, L.; Hope, B. B. Corrosion inhibitors in concrete – Part I: The principles. *Cement. Concrete. Res.* **1998**, 28, 1775-1781.
- (5) Sastri, V.S, *Corrosion inhibitors: principles and applications*, Willey: England, **1998**.
- (6) Lane, D.R.; Melendez, J.A.; Munteanu, V.F.; Kinney, F.D. Corrosion inhibiting admixture for concrete. *US Patent* **2002**, 6,340, 438.
- (7) Trépanier, S. M.; Hope, B. B.; Hansson, C. M. Corrosion inhibitors in concrete. Part III. Effect on time to chloride-induced corrosion initiation and subsequent corrosion rates of steel in mortar. *Cement. Concrete. Res.* **2001**. 31, 713-718.
- (8) Stratfull, R. F. The corrosion of steel in a reinforced concrete bridge. *Corrosion* **1957**, 13, 173-179
- (9) Craig, R. J.; Wood, L. E. Effectiveness of corrosion inhibitors and their influence on the physical properties of Portland cement mortars. *Highway Res. Rec.* **1970**, 328:77
- (10) Saricimen, H.; Mohammad, M.; Quddus, A.; Shameem, M.; Barry, M. S. Effectiveness of concrete inhibitors in retarding rebar corrosion. *Cement. Concrete. Comp.* **2002**, 24, 89-100.

- (11) Dhouibi, L.; Triki, E.; Raharinaivo, A. The application of electrochemical impedance spectroscopy to determine the long-term effectiveness of corrosion inhibitors for steel in concrete. *Cement. Concrete. Res.* **2002**, 24, 35-43.
- (12) Yunovich, M.; Thompson, N. G. Performance of corrosion inhibiting admixtures for structural concrete - assessment methods and predictive modeling, Corrosion NACEExpo 98, NACE International, San Diego, CA. **1998**, Paper No. 655.
- (13) Monticelli, C.; Frignani, A.; Trabanelli, G.; Brunoro, G. A study on the inhibiting efficiency of a glycerophosphate-nitrite admixture against steel corrosion in mortars. Proceedings of the 8th European Symposium on Corrosion Inhibitors. University of Ferrara, Ferrara, Italy. **1995**, 1, 609-620.
- (14) Monticelli, C.; Frignani, A.; Trabanelli, G. A study on corrosion inhibitors for concrete application. *Cement. Concrete. Res.* **2000**, 30(4), 635-642.
- (15) Monticelli, C.; Frignani, A.; Trabanelli, G. Corrosion inhibition of steel in chloride-containing alkaline solutions. *J. Appl. Electrochem.* **2002**, 32(5), 527-535.
- (16) Welle, A.; Liao, J. D.; Kaiser, K.; Grunze, M.; Blank, N.; Mäder, U. Interactions of N,N'-dimethylaminoethanol with steel surfaces in alkaline and chlorine containing solutions. *Appl. Surf. Sci.* **1997**, 119, 185-198.
- (17) Yang, Z.; Shi, X.; Nguyen, T. A.; Suo, Z.; Avci, R. Corrosion and inhibition performances at the steel-mortar interface. Part 1: A surface analytical investigation. *Ind. Eng. Chem. Res.*, under review.
- (18) Trabanelli, G.; Monticelli, C.; Grassi, V.; Frignani, A. Electrochemical study on inhibitors of rebar corrosion in carbonated concrete. *Cement. Concrete. Res.* **2005**, 35, 1804– 1813.

- (19) Song, S. Application of AC electrochemical spectroscopy (EIS) in the study of corrosion of reinforced concrete. Proceedings of Corrosion and Prevention. November 23-25, 1998, Hobart, Australia. **1998**, 257-264.
- (20) He, X.; Shi, X. Chloride permeability and microstructure of Portland cement mortars incorporating nanomaterials. *Transport. Res. Rec.* **2008**, in press.
- (21) Brown, M. C. Assessment of commercial corrosion inhibiting admixtures for reinforced concrete. Thesis for Master of Science in Civil and Environmental Engineering, Virginia Polytechnic Institute and State University. **1999**.

List of Figures and Tables

Figure 1. EIS Nyquist diagram for sample A: a) complete diagram of 30 kHz -0.005 Hz; b) high frequencies

Figure 2. EIS Nyquist diagram for: a) sample B; and b) sample C; and c) sample D, 30 kHz -0.005 Hz

Figure 3. EIS Nyquist diagram for sample E: a) complete diagram of 30 kHz -0.005 Hz; b) high frequencies

Figure 4. EIS Nyquist diagram for sample F: a) complete diagram of 30 kHz -0.005 Hz; b) high frequencies

Figure 5. Equivalent electric circuit for the steel-mortar system under salt ponding

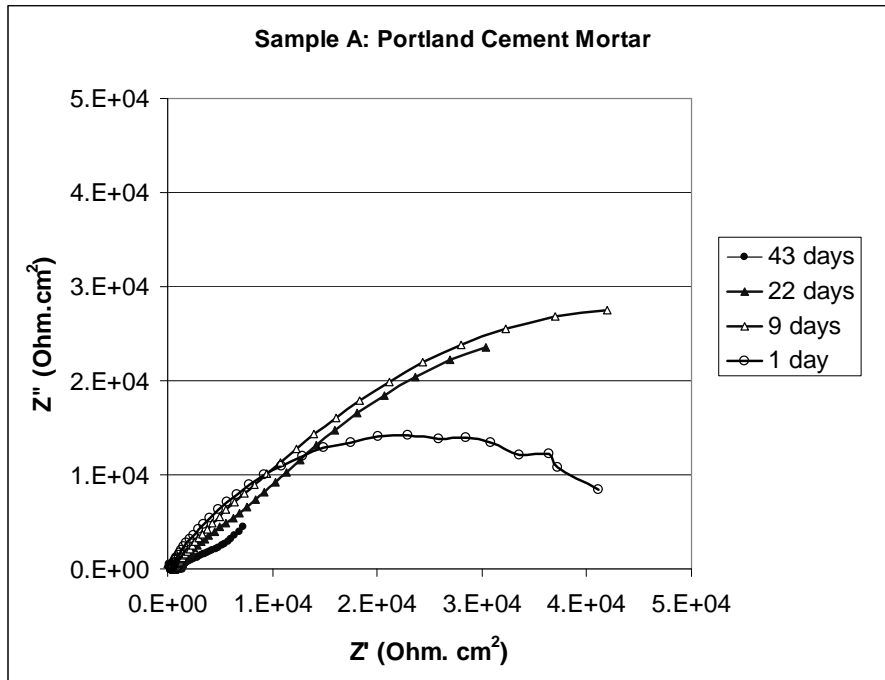
Figure 6. Evolution of R_0 (a) and C_0 (b) over time for steel-mortar sample under salt ponding

Figure 7. Evolution of R_1 (a) (b) and C_1 (c) over time for steel-mortar sample under salt ponding

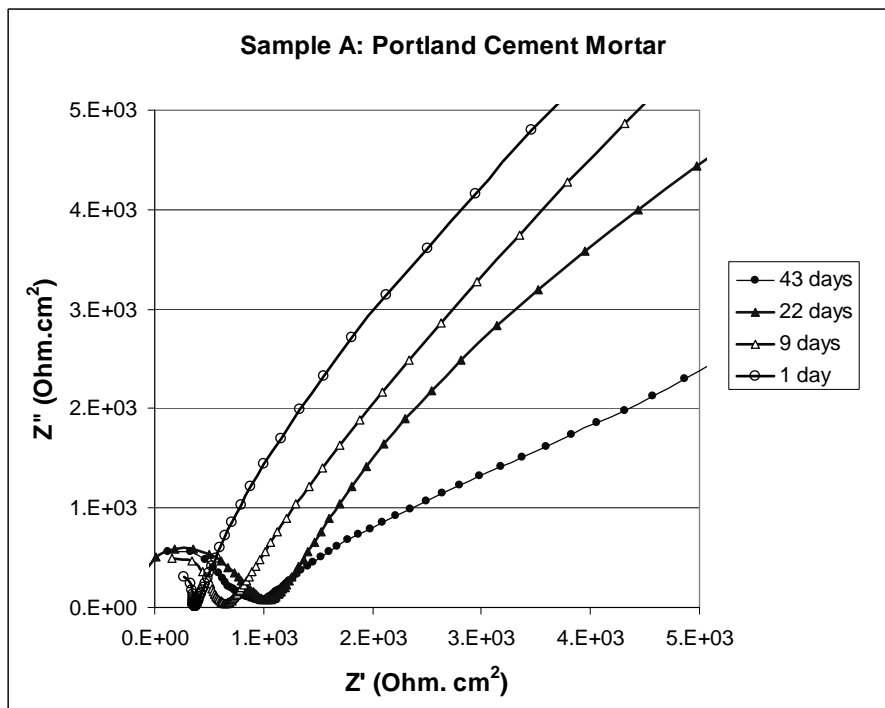
Figure 8. Corrosion current density of steel as a function of mix design and salt ponding time

Figure 9. Evolution of OCP of the steel over time for: a) samples with or without admixed NaCl; and b) samples with or without admixed corrosion inhibitors

Table 1. Mix design of mortar samples investigated (percentages and concentrations were by weight of water)

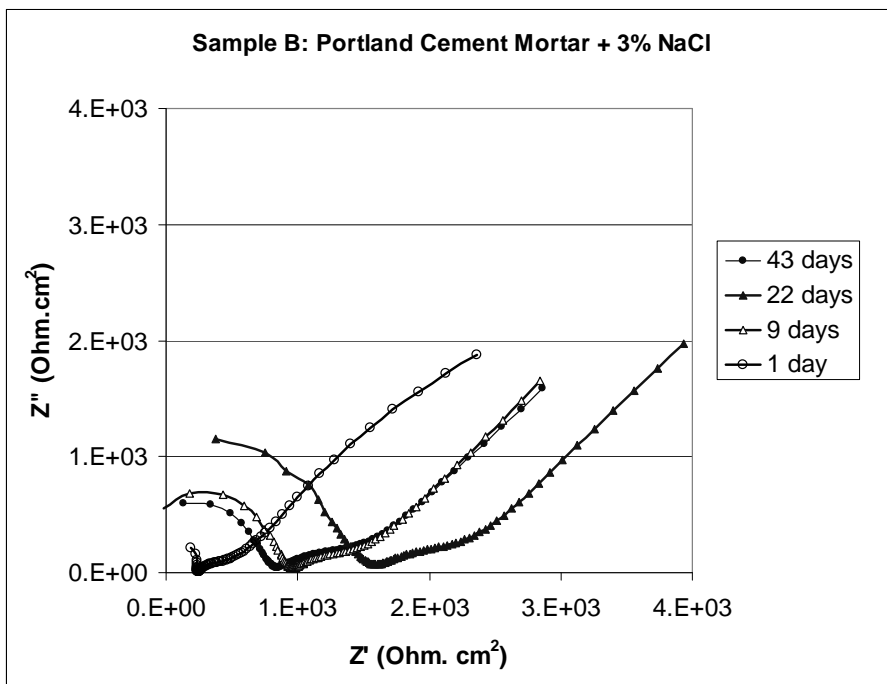


(a)

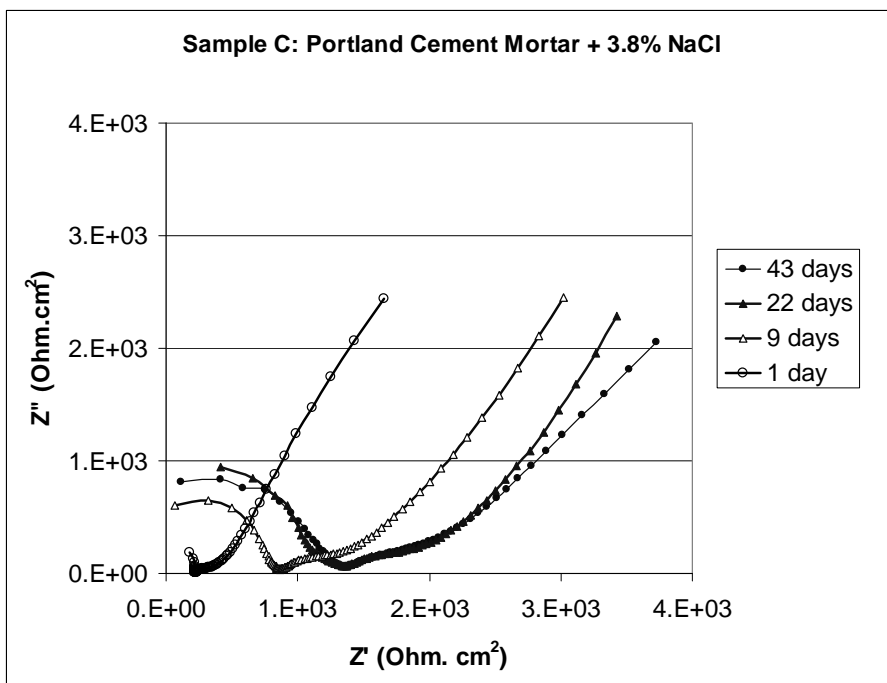


(b)

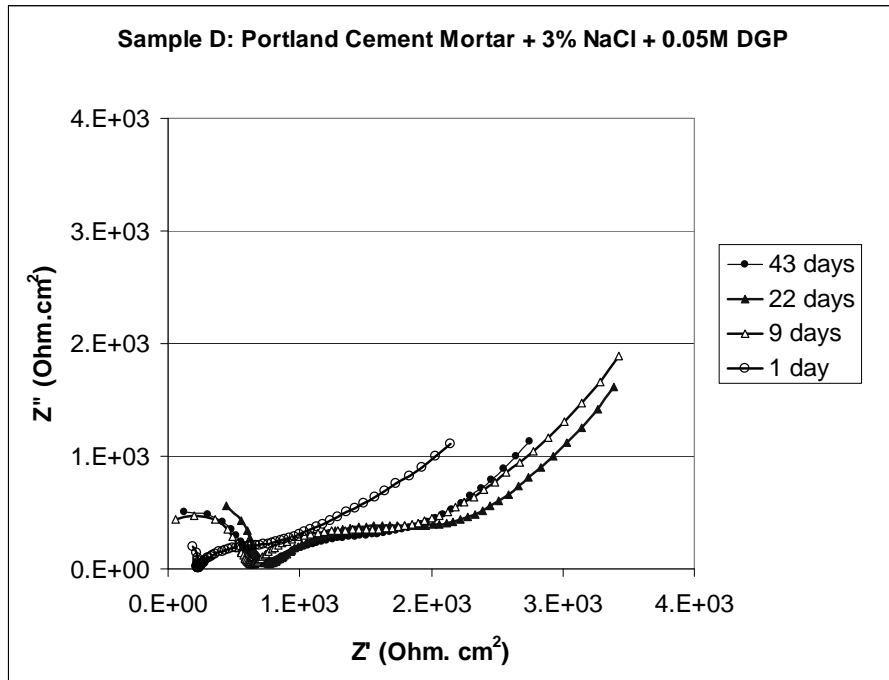
Figure 1.



a)



b)



c)

Figure 2.

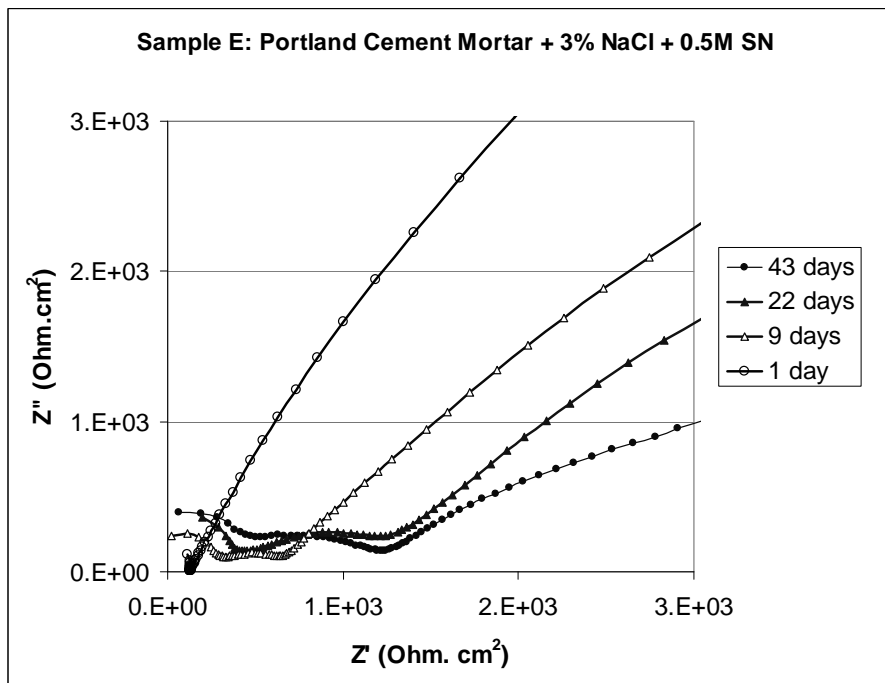
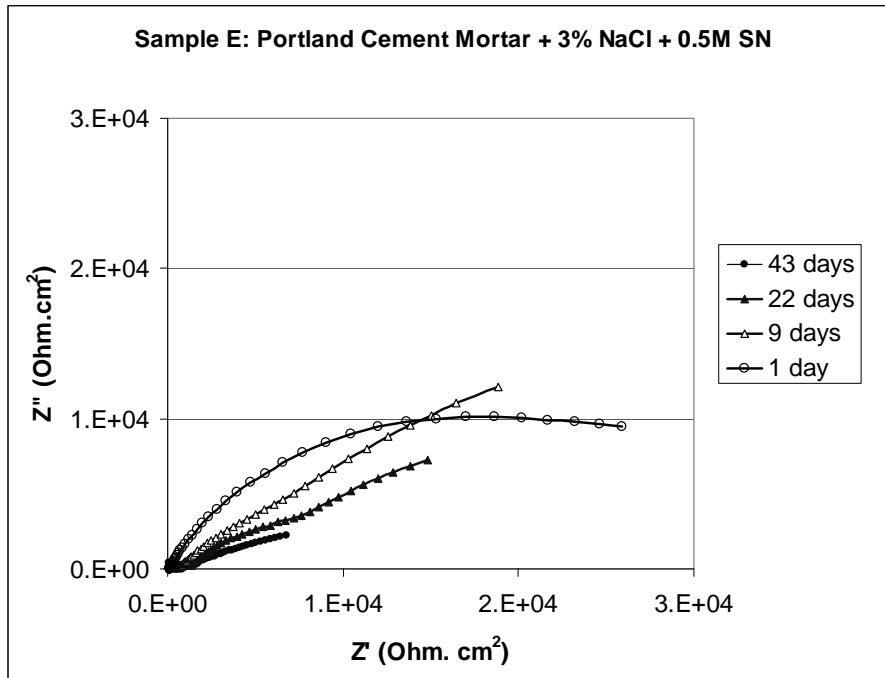


Figure 3.

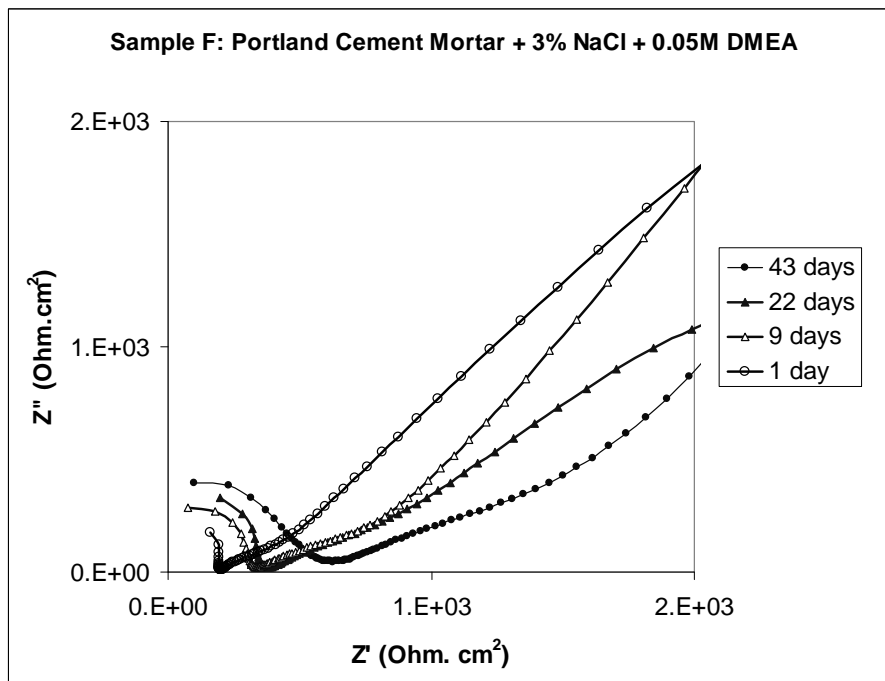
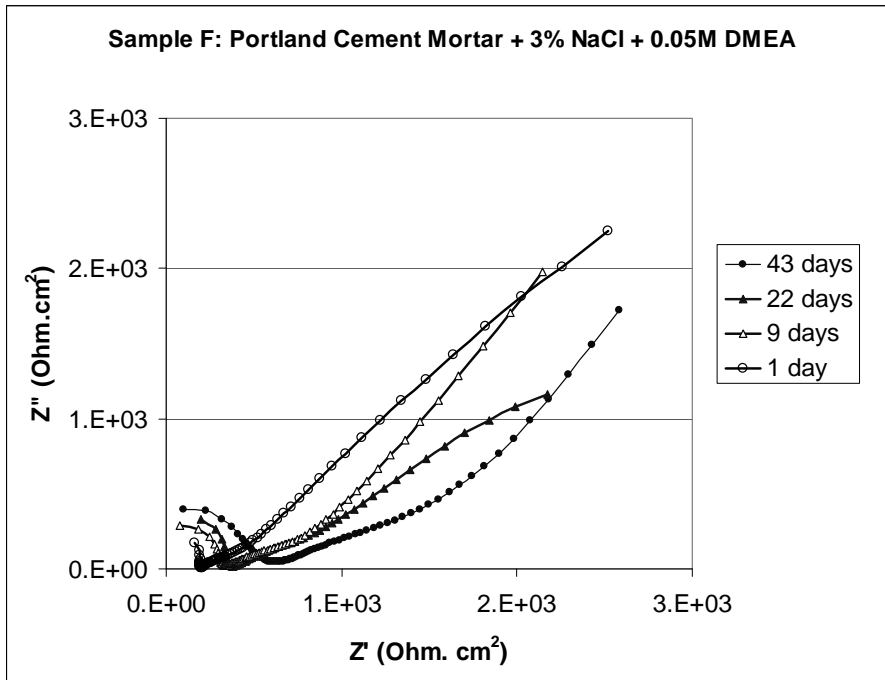


Figure 4.

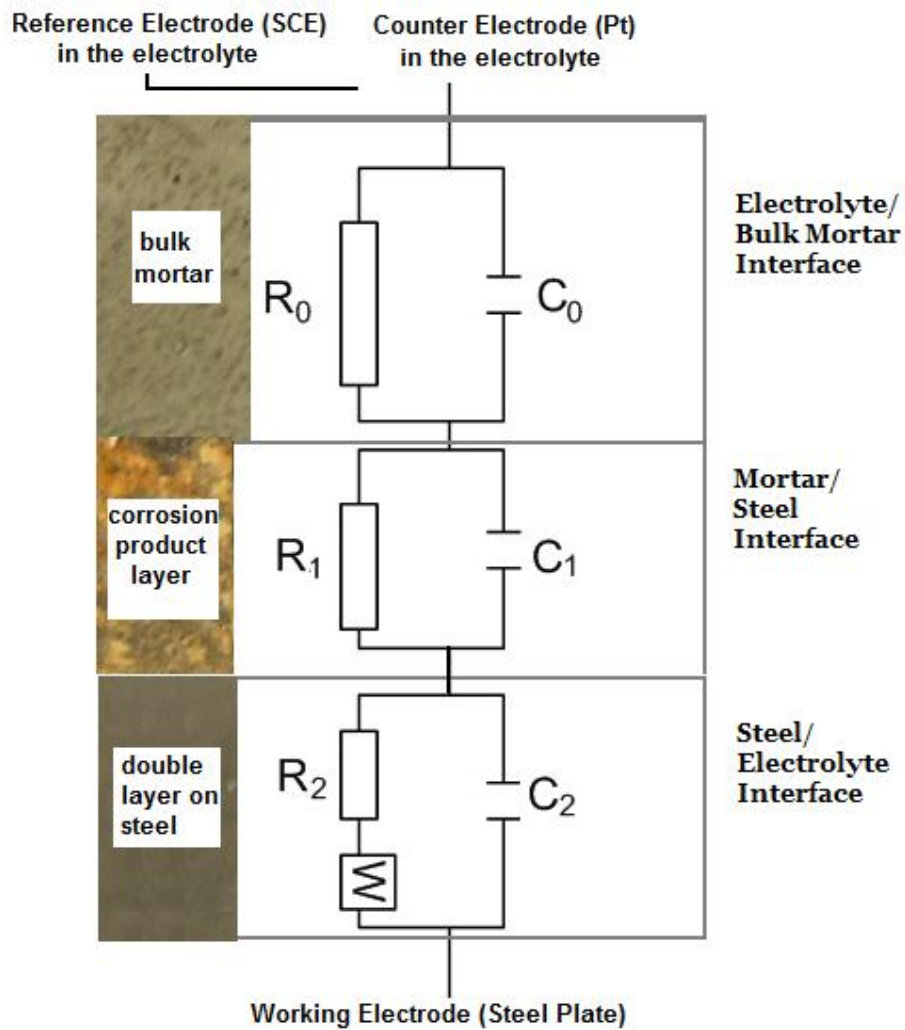
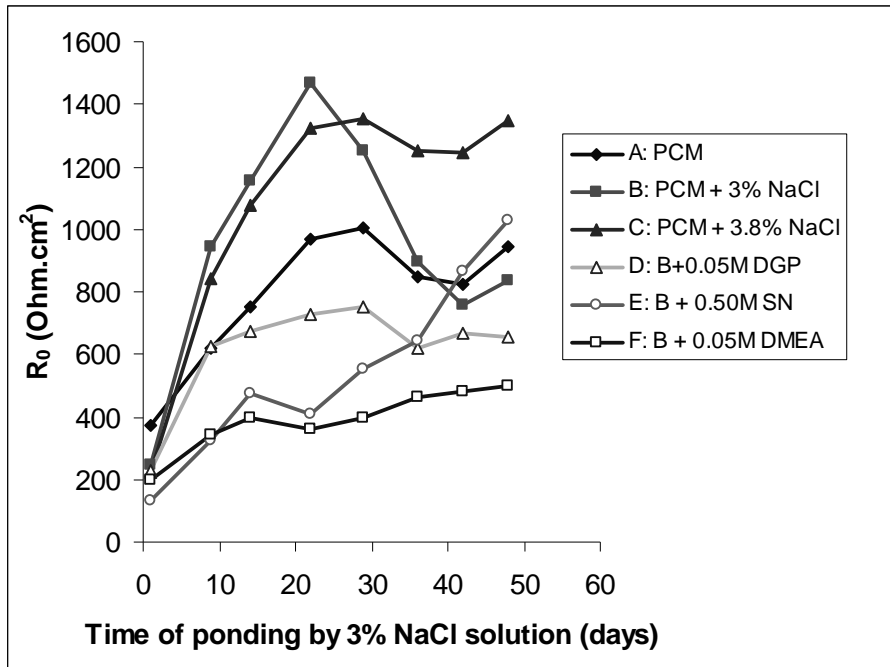
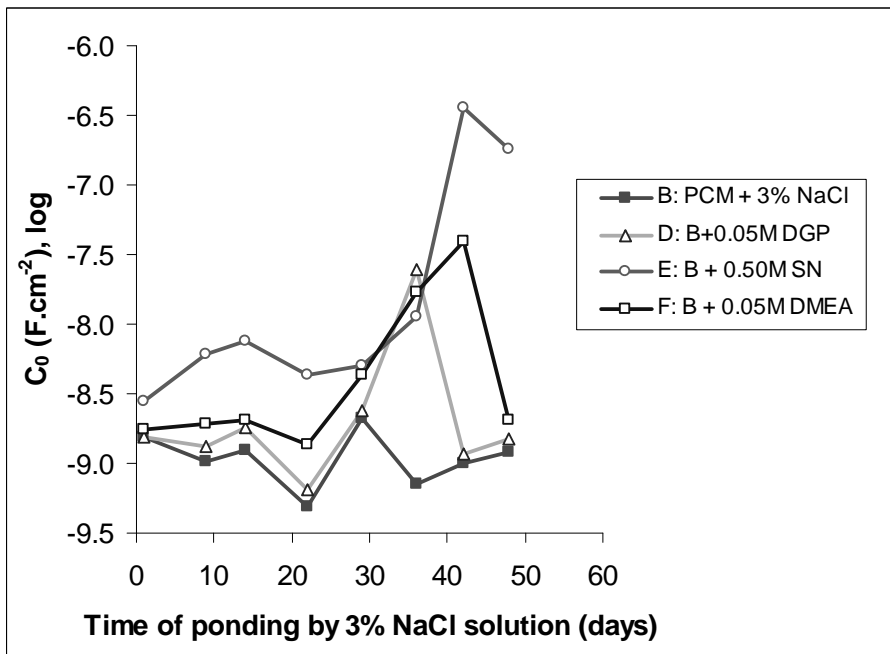


Figure 5.

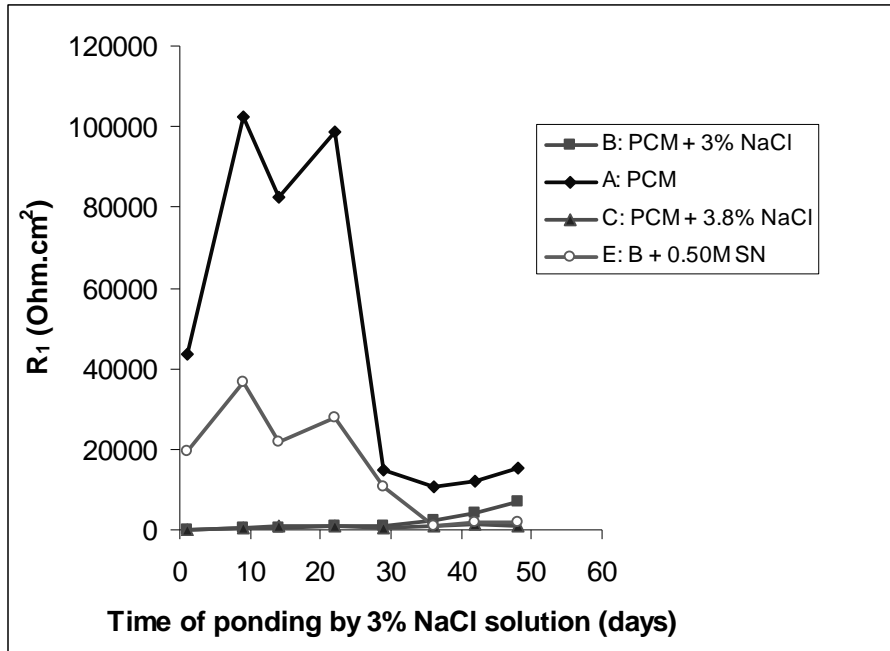


(a)

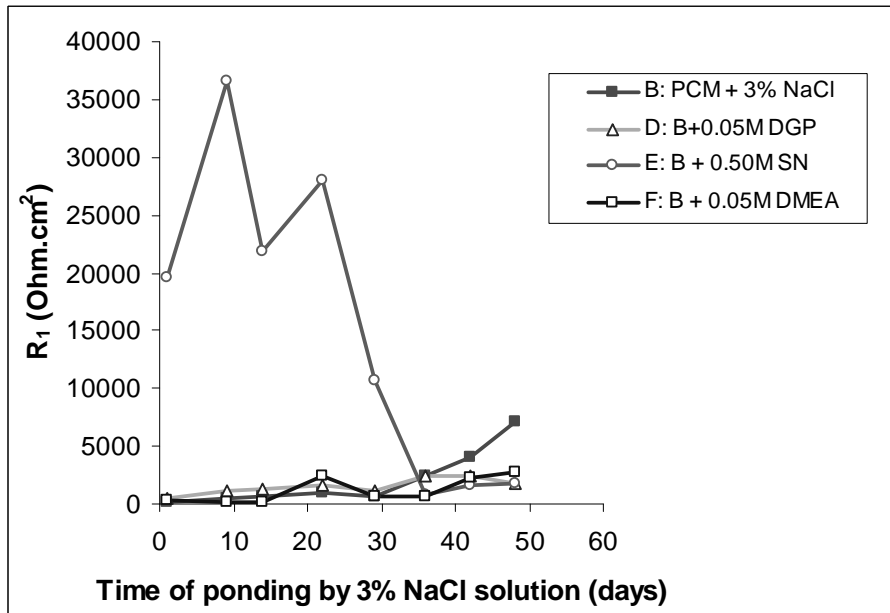


(b)

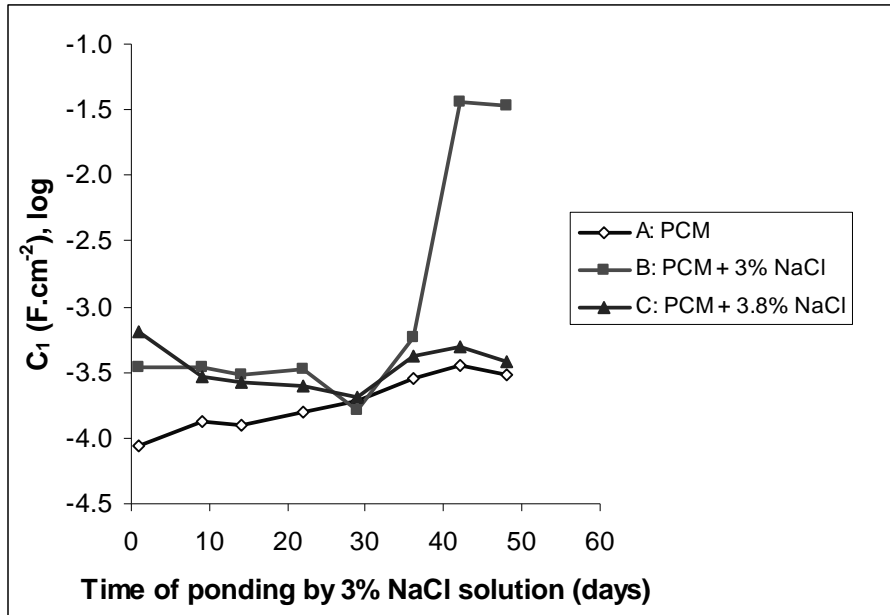
Figure 6.



(a)



(b)



(c)

Figure 7.

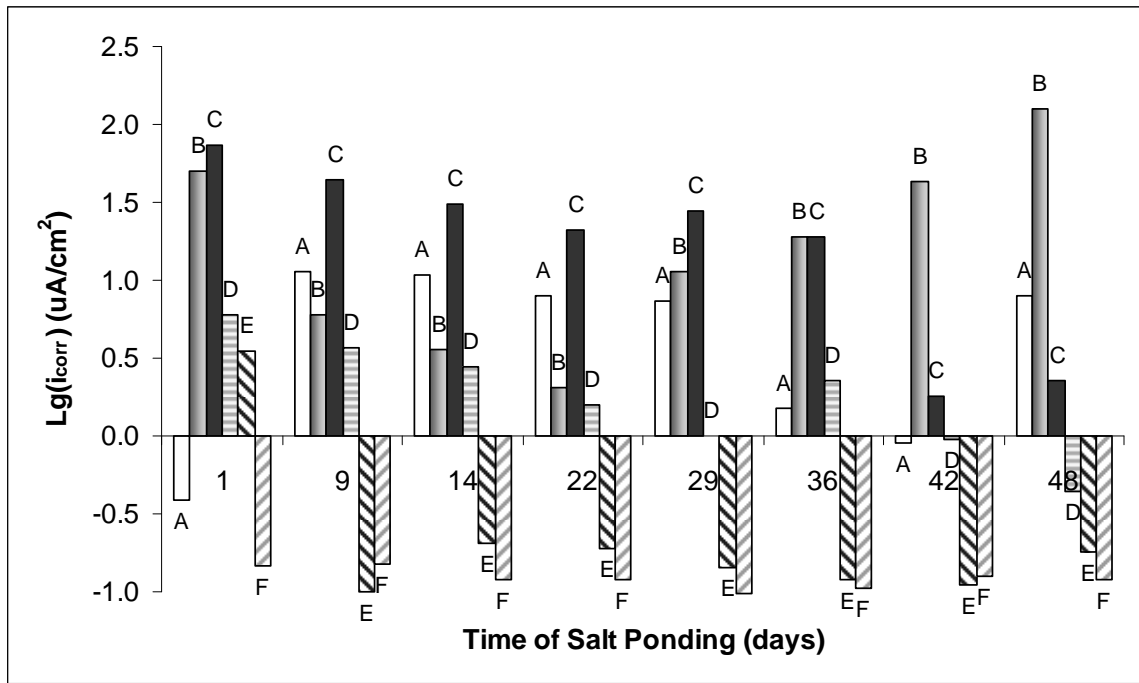
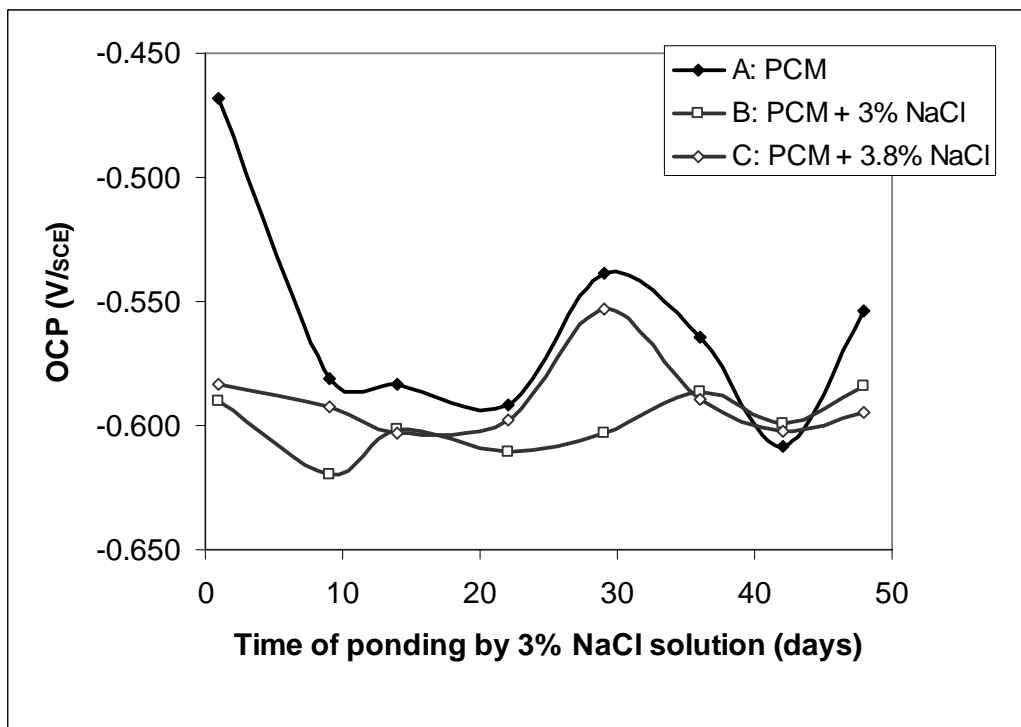
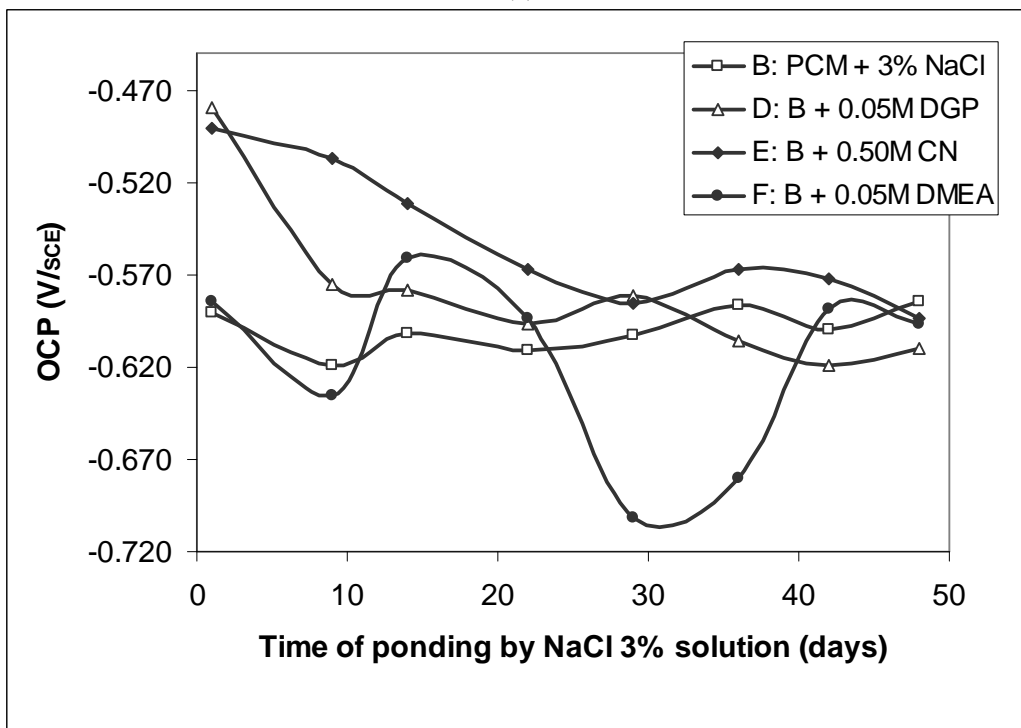


Figure 8.



(a)



b)

Figure 9.

Table 1.

Samples	A	B	C	D	E	F
Cement	×	×	×	×	×	×
Sand	×	×	×	×	×	×
Water	×	×	×	×	×	×
3% NaCl		×		×	×	×
3.8% NaCl			×			
0.05M DGP				×		
0.5M SN					×	
0.05M DMEA						×